Department of Applied Physics

Thermochemical and thermomechanical modeling of nuclear fuel

Henri Loukusa

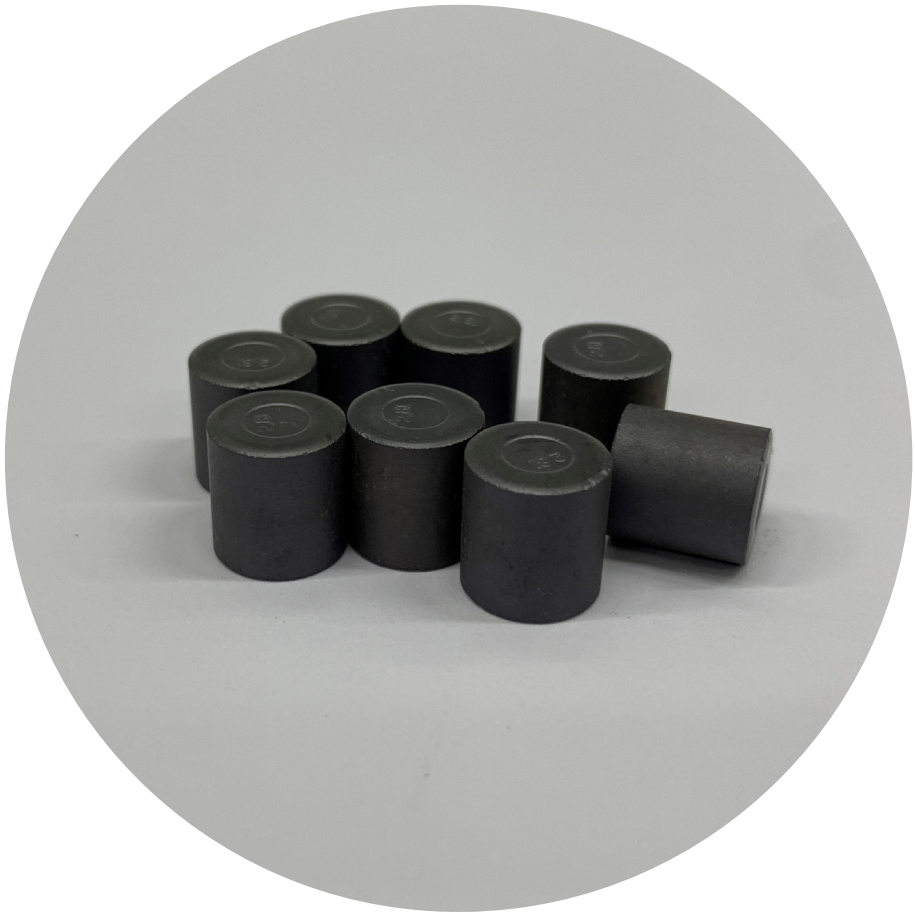

Aalto University

DOCTORAL DISSERTATIONS

Aalto University publication series
DOCTORAL DISSERTATIONS 22/2020

Thermochemical and thermomechanical modeling of nuclear fuel

Henri Loukusa

A doctoral dissertation completed for the degree of Doctor of Science (Technology) to be defended, with the permission of the Aalto University School of Science, at a public examination held at the lecture hall E of the school on 28 February 2020 at 13:00.

Aalto University
School of Science
Department of Applied Physics

Supervising professor
Prof. Filip Tuomisto, Aalto University, Finland

Thesis advisors
Dr. Ville Tulkki, VTT Technical Research Centre of Finland Ltd.
Dr. Timo Ikonen, VTT Technical Research Centre of Finland Ltd.

Preliminary examiners
Prof. Markus Piro, Ontario Tech University, Canada
Dr. Giovanni Pastore, Idaho National Laboratory, United States

Opponent
Dr. Jerome Sercombe, Commissariat à l'énergie atomique et aux énergies alternatives, France

Aalto University publication series
DOCTORAL DISSERTATIONS 22/2020

ISBN 978-952-60-8942-3 (printed)
ISBN 978-952-60-8943-0 (pdf)
ISSN 1799-4934 (printed)
ISSN 1799-4942 (pdf)
http://urn.fi/URN:ISBN:978-952-60-8943-0

Unigrafia Oy
Helsinki 2020

Finland

Printed matter
4041-0619

Aalto University

Abstract

Aalto University, P.O. Box 11000, FI-00076 Aalto www.aalto.fi

Author
Henri Loukusa

Name of the doctoral dissertation
Thermochemical and thermomechanical modeling of nuclear fuel

Publisher School of Science

Unit Department of Applied Physics

Series Aalto University publication series DOCTORAL DISSERTATIONS 22/2020

Field of research Engineering Physics

Manuscript submitted 20 September 2019 **Date of the defence** 28 February 2020

Permission for public defence granted (date) 17 December 2019 **Language** English

☐ **Monograph** ☒ **Article dissertation** ☐ **Essay dissertation**

Abstract

Nuclear fuel undergoes various changes in its properties and composition as it is irradiated in a nuclear power plant. Typical light-water reactor fuel consists of ceramic uranium oxide pellets encased in a zirconium alloy tube called the cladding. As actinide atoms are fissioned, the elemental composition of the pellets change as fission products form. Irradiation damage is accumulated and the pellets expand due to the accumulation of fission products. The cladding also experiences irradiation damage, and undergoes mechanical deformation during irradiation due to a pressure differential between the inside of the rod and the coolant and mechanical interaction with the expanding pellet.

The effects of the composition change on the chemical properties are studied in this thesis with thermochemical modeling using Gibbs energy minimization. Especially the oxygen potential of the pellets is studied, as it is a general indicator of the oxidation state and relatively easily measurable experimentally. Validation of the oxygen potential predictions is performed against experimental data from the literature for fresh and irradiated fuel. In addition, the release of corrosive gases from the pellet is studied, as they may affect cladding crack formation.

The FINIX fuel behavior module has been developed at VTT for multiphysics applications, and in this thesis its thermomechanical modeling capabilities are extended to cover long irradiation periods. Several models of important phenomena that occur during long irradiations were not present in FINIX, but were implemented as part of this thesis in order to improve the temperature predictions of FINIX. As a result of this development, the temperature predictions during long irradiations have improved substantially in accuracy.

Additionally, uncertainty analysis based on the order statistics method was performed on fission gas release predictions of the ENIGMA fuel performance code. Fission gas release can be correlated with the instant release fraction of some radionuclides in spent fuel disposal. The instant release fraction is the fraction of radionuclides that are released relatively instantly as groundwater becomes in contact with the fuel after the disposal canister has failed. With an estimate of the uncertainty of the fission gas release predictions, the uncertainty of the instant release fraction can be studied in more detail.

Keywords nuclear fuel behavior, thermochemistry, thermomechanics, uncertainty analysis

ISBN (printed) 978-952-60-8942-3 **ISBN (pdf)** 978-952-60-8943-0

ISSN (printed) 1799-4934 **ISSN (pdf)** 1799-4942

Location of publisher Helsinki **Location of printing** Helsinki **Year** 2020

Pages 169 **urn** http://urn.fi/URN:ISBN:978-952-60-8943-0

Tekijä
Henri Loukusa

Väitöskirjan nimi
Ydinpolttoaineen termokemiallinen ja termomekaaninen mallinnus

Julkaisija Perustieteiden korkeakoulu

Yksikkö Teknillisen fysiikan laitos

Sarja Aalto University publication series DOCTORAL DISSERTATIONS 22/2020

Tutkimusala Teknillinen fysiikka

Käsikirjoituksen pvm 20.09.2019 **Väitöspäivä** 28.02.2020

Väittelyluvan myöntämispäivä 17.12.2019 **Kieli** Englanti

☐ **Monografia** ☒ **Artikkeliväitöskirja** ☐ **Esseeväitöskirja**

Tiivistelmä

Ydinpolttoaineen materiaaliominaisuuksissa ja koostumuksessa tapahtuu erilaisia muutoksia säteilytyksen aikana. Tavallinen kevytvesireaktorin polttoaine koostuu keraamisista uraanidioksidipelleteistä zirkoniummetalliseoksesta tehdyn suojakuoriputken sisällä. Kun aktinidiatomit fissioituvat, polttoainepellettien alkuainekoostumus muuttuu fissiotuotteiden syntyessä, säteilyvaurioita kertyy ja pelletit paisuvat fissiotuotteiden kertymisen johdosta. Myös suojakuoressa kertyy säteilyvaurioita ja suojakuori muuttaa muotoaan johtuen suojakuoren sisä- ja ulkopuolen välillä olevasta paine-erosta ja mekaanisesta vuorovaikutuksesta pelletin kanssa.

Pellettien alkuainekoostumuksen vaikutuksia niiden kemialliseen käyttäytymiseen tutkitaan tässä väitöskirjassa termokemiallisesti Gibbsin energian minimoinnin avulla. Erityistä huomiota annetaan pellettien happipotentiaalille, sillä happipotentiaali kertoo yleisluonteisesti polttoaineen hapetustilasta ja on suhteellisen helposti määritettävissä kokeellisesti. Väitöskirjassa laskettuja happipotentiaaliennusteita kelpoistetaan vertaamalla niitä kirjallisuudesta löytyviin kokeellisesti määritettyihin happipotentiaaleihin tuoreelle ja säteilytetylle polttoaineelle. Lisäksi tarkastellaan syövyttävien kaasujen vapautumista pelletistä, sillä niillä voi olla vaikutusta suojakuoressa tapahtuvaan säröytymiseen.

FINIX-polttoainemalli on kehitetty VTT:llä polttoainemalliksi monifysiikkasovelluksiin, ja tässä väitöskirjassa sen termomekaanista mallinnuskykyä on parannettu. Parannusten jälkeen mallilla on mahdollista mallintaa entistä tarkemmin pitkiä säteilytysjaksoja. Useita malleja ilmiöistä, joita polttoaineessa tapahtuu pitkien säteilytysjaksojen aikana, on puuttunut FINIX-mallista, mutta näitä malleja on toteutettu FINIX-malliin lämpötilaennusteiden tarkentamiseksi osana tätä väitöskirjaa. Lopputuloksena nämä ennusteet ovat tarkentuneet huomattavasti.

Lisäksi väitöskirjassa on kehitetty epävarmuusanalyysimenetelmä fissiokaasujen vapautumisosuuden laskennalle ENIGMA-polttoainekoodilla. Fissiokaasujen vapautumisosuuden voidaan sanoa olevan verrannollinen tiettyjen radionuklidien niin sanottuun välittömään vapautumisosuuteen, jota käytetään loppusijoituslaitoksen turvallisuusanalyyseissä. Välitön vapautumisosuus kertoo sen osuuden radionuklideista jotka liukenevat suhteellisen välittömästi niiden tullessa kosketuksiin pohjaveden kanssa loppusijoituskapselin rikkouduttua. Arviolla fissiokaasujen vapautumisosuuden epävarmuudesta voidaan arvioida tarkemmin välittömän vapautumisosuuden epävarmuutta.

Avainsanat ydinpolttoaineen käyttäytyminen, termokemia, termomekaniikka, epävarmuusanalyysi

ISBN (painettu) 978-952-60-8942-3 **ISBN (pdf)** 978-952-60-8943-0

ISSN (painettu) 1799-4934 **ISSN (pdf)** 1799-4942

Julkaisupaikka Helsinki **Painopaikka** Helsinki **Vuosi** 2020

Sivumäärä 169 **urn** http://urn.fi/URN:ISBN:978-952-60-8943-0

Preface

The work in this thesis has been performed at the VTT Technical Research Centre of Finland Ltd. in the Reactor analysis team.

The work on the FINIX fuel behavior module has been funded by the Finnish Research Programmes on Nuclear Power Plant Safety SAFIR2014 (2010-2014) in the PALAMA project, SAFIR2018 (2015-2018) in the PANCHO project and SAFIR2022 (2019-2022) in the INFLAME project. I have also received two personal grants from the Fortum Foundation and contributed to the IDEA project of the Academy of Finland (grant decision number 260493), which enabled the part of the thesis focused on nuclear fuel thermochemistry. I am also grateful for Teollisuuden Voima Oyj and Posiva Oy, who kindly have given the permission to publish the analysis method presented in Publication VI.

I would like to thank my thesis advisors Timo Ikonen and Ville Tulkki, who I was able to count on for advice, and Filip Tuomisto for acting as supervising professor for this thesis. Stimulating discussions with many colleagues at the Nuclear energy research area at VTT have also aided me in performing the work in this thesis. I also appreciate help from Pertti Koukkari and coworkers at VTT on the subject of Gibbs energy minimization.

I would also like to thank my friends and family for support during this project, especially my wife Inari.

Helsinki, January 20, 2020,

Henri Loukusa

Contents

List of Publications

This thesis consists of an overview and of the following publications which are referred to in the text by their Roman numerals.

I Henri Loukusa, Timo Ikonen, Antti Räty, Ville Tulkki. Thermochemical modelling of the oxygen potential of uranium oxide fuel pellets under irradiation. In *TopFuel*, Zürich, Switzerland. Article A0005, September 2015.

II Henri Loukusa, Timo Ikonen, Ville Valtavirta, Ville Tulkki. Thermochemical modeling of nuclear fuel and the effects of oxygen potential buffers. *Journal Of Nuclear Materials*, Volume 481, pages 101-110, December 2016.

III Henri Loukusa, Ville Valtavirta. Application of constrained Gibbs energy minimization to nuclear fuel thermochemistry. In *TopFuel*, Prague, Czechia. Article A0127, October 2018.

IV Timo Ikonen, Henri Loukusa, Elina Syrjälahti, Ville Valtavirta, Jaakko Leppänen, Ville Tulkki. Module for thermomechanical modeling of LWR fuel in multiphysics simulations. *Annals of Nuclear Energy*, Volume 84, pages 111-121, November 2014.

V Henri Loukusa, Jussi Peltonen, Ville Valtavirta, Ville Tulkki. Implementation of burnup effects in the multiphysics fuel behavior module FINIX. *Annals of Nuclear Energy*, Volume 36, paper 107022, 2020.

VI Henri Loukusa, Ville Tulkki. Determination of tolerance limits for fuel assembly fission gas release summary statistics. *Nuclear Engineering and Design*, Volume 358, paper 110438, 2020.

Author's Contribution

Publication I: "Thermochemical modelling of the oxygen potential of uranium oxide fuel pellets under irradiation"

The author was the primary author of the paper and performed the development of the thermochemical equilibrium solver, and thermochemical and thermomechanical calculations and analyses.

Publication II: "Thermochemical modeling of nuclear fuel and the effects of oxygen potential buffers"

The author was the primary author of the paper and performed the thermochemical and thermomechanical calculations and analyses.

Publication III: "Application of constrained Gibbs energy minimization to nuclear fuel thermochemistry"

The author was the primary author of the paper, performed the development of the radiolysis model and the thermochemical and chemical kinetic calculations and analyses.

Publication IV: "Module for thermomechanical modeling of LWR fuel in multiphysics simulations"

The author performed the verification and validation of FINIX, and participated in writing section 3 of the paper.

Publication V: "Implementation of burnup effects in the multiphysics fuel behavior module FINIX"

The author was the primary author of the paper, and performed the implementation of cladding plasticity and creep models as well as radial power distribution, pellet swelling and densification and fission gas release models in FINIX.

Publication VI: "Determination of tolerance limits for fuel assembly fission gas release summary statistics"

The author was the primary author of the paper, and performed the development of the method and the calculations presented in the paper.

Abbreviations

BISON A fuel performance code developed at the Idaho National Laboratory in the US

BWR Boiling water reactor

CANDU Canada Deuterium Uranium, a pressurized heavy water reactor

EPMA Electron probe microanalysis

ENIGMA A fuel performance code originally developed by Nuclear Electric in the UK

% FIMA percent fissioned initial metal atoms

FINIX Fuel behavior model and interface for multiphysixs applications developed at VTT

FRAPCON A steady-state fuel performance code developed by the Pacific Northwest National Laboratory for the US NRC

FRAPTRAN A transient fuel performance code developed by the Pacific Northwest National Laboratory for the US NRC

GEM Gibbs energy minimization

hcp hexagonal close packed

IAEA International Atomic Energy Agency

IFA Instrumented Fuel Assembly

IFPE International Fuel Performance Experiments database

IRF Instant Release Fraction

LWR Light-water reactor

MFPR A mesoscale fuel performance code developed by IBRAE in Russia and IRSN in France

NPP Nuclear power plant

OECD/NEA Nuclear Energy Agency of the Organisation for Economic Co-operation and Development

PCI Pellet-cladding interaction

PWR Pressurized water reactor

RFTT RMC Fuel Thermochemical Treatment

Serpent Monte Carlo neutronics code developed at VTT

SOLGASMIX A Gibbs energy minimization program

STUK Säteilyturvakeskus, Finnish Radiation and Nuclear Safety Authority

TRANSURANUS A fuel performance code developed by the Institute of Transuranium Elements, a Joint Research Center of the European Union

TUBRNP TRANSURANUS burnup equations model

US NRC United States Nuclear Regulatory Commission

Symbols

β confidence

γ probability content

γ_i activity coefficient

Γ_j Lagrange coefficient

ϵ_θ hoop strain

ϵ_c creep strain

ϵ_{c1} primary creep strain

ϵ_{c2} secondary creep strain

ϵ_e effective strain

λ thermal conductivity

μ chemical potential

μ^p chemical potential of a pure species

$\tilde{\mu}$ reduced chemical potential, $\frac{\mu}{RT}$

ν Poisson's ratio

ξ extent of reaction

σ_θ hoop stress

σ_e effective stress

σ_Y yield strength

σ_z axial stress

ϕ particle flux or index over phases

A Helmholtz free energy or affinity

A_{gb} average area of a grain boundary bubble

$\mathbf{A}$ stoichiometric matrix

a_{ij} stoichiometric coefficient

B burnup

b rate of irradiation-induced redissolution of gas atoms

b_j constraint

$\mathbf{b}$ constraint vector

C number of components

C_p isobaric heat capacity

C_v isochoric heat capacity

$D_{\mathbf{atom}}$ diffusion coefficient of fission gases

$D_{\mathbf{bubble}}$ diffusion coefficient of fission gas bubbles

$D_{\mathbf{eff}}$ effective diffusion coefficient of fission gases

E elastic modulus or fission fragment energy

E_0 initial energy of fission fragment

f_E probability density function of fission fragment energies

F degrees of freedom

F_c fractional coverage of grain boundaries by bubbles

$\dot{F}$ fission rate

G Gibbs energy

g trapping rate of gas atoms into intragranular bubbles

G^{ex} excess Gibbs energy

G_i partial molar Gibbs energy

H enthalpy

h pellet-cladding gap conductance

$h_{\mathbf{cond}}$ pellet-cladding gap conduction conductance

$h_{\mathbf{rad}}$ pellet-cladding gap radiative conductance

$h_{\mathbf{contact}}$ pellet-cladding gap contact conductance

H^{ex} excess enthalpy

H^{p} enthalpy of a pure species

H_f° enthalpy of formation at standard state

ΔH_{tr} enthalpy change of phase transition

k_i reaction rate constant

l characteristic length

n mole amount

$\mathbf{n}$ mole amount vector

N number of simulation runs

N_{gb} number density of grain boundary bubbles

P number of phases

p pressure

p_{hs} hydrostatic pressure

q heat flux

R gas constant

R_{ff} range of fission fragment

r radius

r_{ci} cladding inner radius

r_{co} cladding outer radius

r_f fuel pellet radius

S entropy

S° entropy at standard state

S^{ex} excess entropy

ΔS_{tr} entropy change of phase transition

S^{p} entropy of a pure species

s_i deviatoric stress

T temperature

t time

U internal energy

V volume

V_m molar volume

x_i mole fraction or sample

y_i order statistic

Y fission yield

Z general thermodynamic potential

Z_i partial molar general thermodynamic potential

1. Introduction

1.1 Nuclear fuel

Nuclear fuel is the most central part of the nuclear power plant. In the process of heat generation within the fuel, radioactive nuclides form within the fuel through fission of actinides and combine with each other and the actinide fuel to form various compounds. In typical light water reactors (LWR), the fuel pellets containing most of the radioactive nuclides are situated within a metallic cladding tube, which is typically made out of a zirconium alloy. In between the fuel pellets and the cladding, a gap is present containing a thermally conductive gas, typically helium. To be able to operate a nuclear power plant, the integrity of the cladding must be maintained to prevent the release of these radioactive nuclides. The fuel matrix is typically thought as the first release barrier of radioactive material and the cladding the second barrier. In addition, the primary circuit and containment building are the next barriers should the cladding fail.

Within the reactor, the fuel is subjected to extreme conditions of high temperature, a high temperature gradient and a high radiation field. High energy particle radiation causes the most damage, and the particles causing most damage to the fuel microstructure are neutrons and fission fragments. Fission fragments are the nuclei of the elements formed in fission, and carry a part of the energy released in fission as their kinetic energy. In the cladding, it is neutrons that mostly cause irradiation damage, but in the fuel pellet fission fragments are the most energetic particles [1]. Due to these extreme conditions, over time the properties of the fuel change, typically negatively: for example, the thermal conductivity decreases and the temperature of the fuel increases, the cladding hardens and may become brittle due to hydride formation, the pellet cracks due to the steep temperature gradient and gaseous fission products form within the fuel which may increase the internal pressure of the rod upon release to the rod free volume.

In typical light water reactor fuel, this aging of fuel can be quantified with

burnup, which is a measure of produced energy per unit mass of the actinide used as fuel. A typical unit of burnup is $\mathrm{MWd \cdot kg_U^{-1}}$, megawatt-days per kilogram of uranium. With the energy released per fission, burnup can also be converted to percent fissioned initial metal atoms (% FIMA). % FIMA is typically used instead of burnup in fast reactors, for example. In fast reactors, the neutrons on average have higher energies than thermal reactors such as LWRs. Finally, in materials technology, displacement per atom (dpa) is often used, which is the number of times an average atom is displaced from its site in a crystal lattice. As more energy is produced in the fuel, the more actinide atoms have been fissioned. Even though the measure of burnup as a measure is quite exotic, it can easily be related to such parameters as elemental composition of the fuel, which is more evident from the measure of % FIMA.

1.2 Fuel chemistry

In fuel behavior modeling, the properties of the fuel are described with various material property models. These models, typically called correlations, often use burnup as a measure of the change in properties of the fuel under irradiation. This is a simplification, as some changes could be attributed to composition change, others to irradiation, and yet others to varying temperature conditions. In cladding material models, this is typically evident in that irradiation is taken into account through the fast neutron flux and its time integral, fluence. In pellet material models the effect of irradiation and composition change are typically bundled in burnup. In practice, the use of such models is simple and efficient, but may lack in accuracy.

The composition change results from fission producing two – or rarely three – fission products and a number of neutrons. The elements formed from fission are not always the same, but form various elements depending on the fissioning nuclide. For ^{235}U, the fission products form with a mass number distribution with two peaks: one at around a mass number of 95, and the other at 140. Some of the most abundant elements formed from fission of ^{235}U are xenon, neodymium, palladium, molybdenum, zirconium, ruthenium, barium and cesium, in decreasing order of abundance [2]. Some elements, such as iodine, form in lesser amounts, but are important to fuel behavior due to their chemical properties [3]. In addition to fission products, higher actinides such as plutonium, americium and curium form in the fuel due to neutron capture beginning with ^{238}U, the most abundant nuclide in typical light-water reactor fuel. In the first part of this thesis, methods to capture the effects of this composition change through thermochemical modeling are presented. The aim of this part of the thesis is to improve methods used to predict the amount of corrosive gases present in the fuel-cladding gap. Modeling the chemical behavior of fission products within the fuel offers a more detailed method to investigate different phenomena in fuel, but especially those heavily dependent on chemistry such as

pellet-cladding interaction where corrosive iodine species threaten the integrity of the cladding [4]. Two parameters are mainly dealt with: the oxygen potential as a general measure of the chemical state of the oxide fuel, and on the other hand the concentrations of corrosive gaseous species in the pellet-cladding gap.

1.3 Fuel behavior modeling

For engineering applications, traditional fuel behavior modeling is the most widely applicable method to investigate fuel behavior. Traditional fuel performance codes typically calculate the temperature distribution and mechanical deformations of the fuel rod, and can be applied in day-to-day use to investigate cladding integrity or fuel melting, for example. Oftentimes this is performed in order to show compliance with regulatory criteria required for these parameters to fulfil. In the second part of this thesis, further development of the FINIX fuel behavior module for multiphysics applications is presented. In multiphysics modeling, several solvers designed to model their respective physical processes are coupled to find a coupled solution, where the solvers provide boundary conditions to each other. A multiphysics approach is beneficial for the accurate analysis of nuclear reactor core, as several different disciplines are required for an accurate solution: neutronics provides the power, fuel behavior solves the temperature of fuel and thermal hydraulics produces the heat transfer out of the fuel and in the coolant. The relationships between these different phenomena are shown in figure 1.1. The fuel behavior model FINIX is designed from the beginning to be used in multiphysics couplings, where different solvers provide their outputs as boundary conditions to other solvers. The main focus of the development in this thesis was the application of models required for simulation of long irradiation periods. The aim of this part of the thesis was to improve especially the temperature predictions of FINIX, as the temperature is the most important parameter passed on to other codes in coupled applications.

The third part of this thesis focuses on uncertainty analysis of fuel behavior and challenges related to spent fuel disposal. As any input parameters to a computational model, and also the parameters of the model, are fundamentally uncertain, the output calculated by such a model has also a degree of uncertainty. For a conservative estimate, limiting values from output value distributions calculated by statistical means can be used instead of best-estimate values to show compliance with regulatory criteria, for example. Fuel performance analysis can yield insight in spent fuel final disposal on the state of spent fuel, and uncertainty analysis can be used to quantify the uncertainty of such predictions. A quite important parameter obtained from fuel performance codes is fission gas release, which can be correlated with the instant release fraction of some of the radionuclides in the spent fuel final repository. The instant release fraction contains nuclides that are thought to release rapidly from damaged disposal canisters, and as such is a limiting factor in the safety case of the

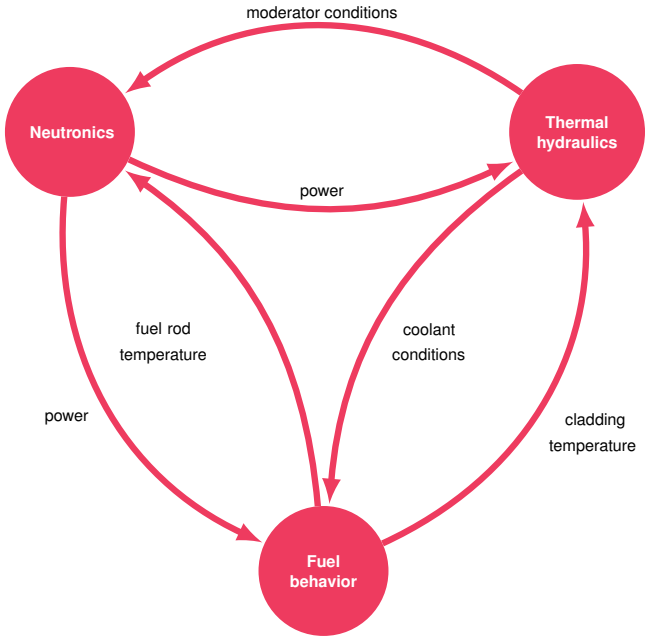

Figure 1.1. The relationship of different models of nuclear reactor core physics. The arrows show the most important calculated parameters that are passed on to other models as boundary conditions. Figure adapted from [5].

spent fuel disposal facility. The aim of the third part of this thesis is to develop a method for the calculation of fission gas release of full reactor cores with associated uncertainty analysis. Such a method is presented in the final part of this thesis.

1.4 Objectives and contributions

The objective of this thesis for the part of nuclear fuel thermochemistry was both to develop a Gibbs energy minimization routine and to apply it to problems related to nuclear fuel. This part of the thesis would not have succeeded without publicly available thermochemical data from the Royal Military College of Canada Fuel Thermochemical Treatment [6]. Unique contributions by the author include the thermochemical solver presented in section 2 and its validation and verification presented in Publications I and II, as well as application of constrained Gibbs energy minimization to cesium iodide radiolysis as presented in Publication III.

For the part concentrating on nuclear fuel behavior modeling and the development of the FINIX multiphysics fuel behavior module, the main focus of this thesis is to increase the prediction accuracy of FINIX under long irradiation

periods. The FINIX fuel behavior module was initially developed by Ikonen [7]. The author has contributed to FINIX development from an early stage, beginning with initial validation efforts [8], which are also reported in Publication IV. The unique contributions of the author regarding the implementation of various models in FINIX are reported in Publication V. The author implemented the cladding plasticity and creep, radial power distribution, fission gas release, pellet swelling and pellet densification models.

In uncertainty analysis of nuclear fuel behavior the objective in this thesis was to develop a method suitable for the calculation of complete reactor cores if necessary, with the specific application to fission gas release. The ENIGMA code [9], developed first by Nuclear Electric in the UK and later modified at VTT, as reviewed by Tulkki [10], was used by the author as the fuel behavior model. The unique contributions of the author include the application of the order statistics method to uncertainty analysis of fuel behavior in normal operation, and the development of the calculation chain. The calculation chain relied on the statistical script originally developed by Ikonen [11], which was modified and developed further by the author to allow for the calculation of full reactor cores.

1.5 Structure

The following chapters are ordered in increasing spatial scale of the studied problem and also in increasing level of abstraction. First, thermochemical behavior of nuclear fuel is covered. In this section, the behavior of nuclear fuel is studied at the microscopic scale. The next section increases the spatial scale of the problem in the nuclear fuel thermomechanical modeling part of this thesis: such modeling describes the macroscopic behavior of complete nuclear fuel rods. In the last section on uncertainty analysis of fuel behavior, the spatial scale is again increased as the uncertainty analysis is performed on complete fuel assemblies containing a hundred or more individual fuel rods. Finally, the findings of the thesis are summarized.

2. Nuclear fuel thermochemistry

2.1 Background

Typical nuclear fuel pellets in light water reactors consist of uranium dioxide, UO_2. Uranium dioxide has a fluorite structure and can exist with considerable nonstoichiometry, e.g. deviation from the exact stoichiometry of two atoms of oxygen per one atom of uranium. Typically, fuel pellets containing only uranium are slightly hyperstoihiometric, that is, contain slightly more than two oxygen atoms per metal atom, which is signified by UO_{2+x}. Hypostoichiometry, where uranium oxide contains less than two oxygen atoms per metal atom, is signified by UO_{2-x}, but this behavior is only found at high temperature for pure uranium dioxide. However, for mixed uranium-plutonium oxide fuel pellets, hypostoichiometry is the norm.

Some other elements are also sometimes present in fuel pellets: burnable neutron absorbers such as gadolinium, or sintering additives chromium or aluminum. These are typically soluble in the uranium dioxide lattice. When the fuel pellet is irradiated, the fissile atoms split into fission products through fission. There are tens of fission product elements that occur in the fuel in macroscopic amounts, and each forms distinct chemical compounds. In thermochemical equilibrium analyses, chemical compounds are often termed species, which may occur as pure species or as solid or liquid solutions with each other.

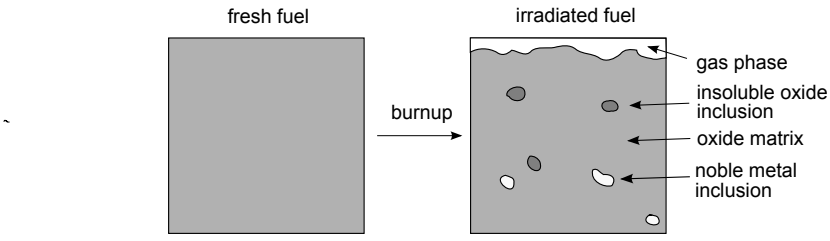

Figure 2.1. The composition change in nuclear fuel under neutron irradiation. Figure drawn after Olander [1], from [12].

Table 2.1. Distribution of fission products to various phases and elemental groups in nuclear fuel, per Kleykamp [13].

Phase	Alkali metals	Alkaline earth metals	Transition metals and lanthanides	Post-transition metals	Metal-loids	Non-metals
Gas phase						Br, I, Kr, Xe
Metallic precipitates			Mo*, Tc, Ru, Rh, Pd, Ag, Cd	In, Sn	Sb, Te	
Oxide precipitates	Rb, Cs	Ba	Zr, Nb, Mo		Te*	
Oxide matrix		Sr	Zr*, Nb*, Y, La, Ce, Pr, Nd, Pm, Sm			

The fission products form approximately uniformly within the fuel grains. In minute amounts most of these are within the uranium dioxide lattice, but as irradiation continues, more and more fission products form and they begin to precipitate into separate phases. Generally, nuclear fuel forms four types of phases [1, 13], and in figure 2.1 this composition change is shown schematically. The major constituent is of course the fluorite oxide matrix consisting mainly of uranium oxide, but several other phases occur in small amounts. These phases are the gas phase, several metallic phases and several more oxide precipitates that are insoluble in the uranium oxide lattice. The fission product elements are typically classified by their preference to appear in these phases, and a classical division by Kleykamp [13] is shown in table 2.1.

The formation of the gas phase has macroscopic effects on the engineering-level behavior of the fuel rod, as is discussed in more detail in section 3. The precipitation of solids from the uranium oxide matrix influences also several phenomena: the precipitation of corrosive substances, such as iodine species, influence the integrity of the cladding trough stress-corrosion cracking [4], and precipitation of geochemically mobile nuclides influences the instant release fraction in spent fuel disposal [14]. Additionally, the presence of certain precipitates can yield information on the chemical state of the fuel in general, such as oxygen potential. Oxygen content itself and free oxygen especially has even been shown to have a preventative effect on cladding crack formation [15, 16].

As is evident from table 2.1, a very large number of fission products form in nuclear fuel, and the number of possible compounds between these fission products and the uranium and oxygen initially in the fuel becomes extremely large. Computational analysis of chemical composition is typically performed

with either chemical kinetics, where the change of composition through chemical reactions is followed in time, or with chemical thermodynamics, which aims to find the chemical composition at thermochemical equilibrium. The first approach requires knowledge of all the important reactions between each chemical species occurring in the system under study. In a system containing as many constituent elements as nuclear fuel, this is practically impossible to have as this would require solving a differential equation system of thousands and thousands of equations with little data for any of the parameters in these equations. On the other hand, finding the thermochemical equilibrium composition only requires knowledge of the thermodynamic potentials of the species occurring in the system. As thermodynamic potentials such as Gibbs energies are readily found tabulated from the literature, this approach is quite feasible.

Often, comprehensive thermochemical data libraries containing these Gibbs energy functions are proprietary. However, there are also public sources of such data. For example, Cordfunke and Konings [17] have published an extensive set of fission product thermochemical data. This data has also been included in the Royal Military College of Canada Fuel Thermochemical Treatment (RFTT) database developed as a database and thermochemical model for CANDU fuel [18, 19, 6, 20], which has been used in this work.

The required data for a thermochemical equilibrium calculation consist of the thermochemical data, the temperature and pressure of the system, but also importantly the elemental composition of the fuel. This elemental composition is conveniently obtained by a burnup calculation performed on the fuel. A typical burnup calculation involves a two-step computation where first the neutron transport equation, a balance equation for neutrons, is solved [21]. The neutron density is used to obtain the reaction rates for neutron-induced nuclear reactions. In the second step of the calculation, constant reaction rates are assumed and the nuclide concentrations are solved from the burnup equations, which form a first-order linear differential equation system [21].

A sample analyzed by Walker et al. [22] was modelled in Publication II, and for that work a burnup calculation for the rod was performed with Serpent [23], a Monte Carlo neutronics code developed at VTT. From this burnup calculation, the mole amounts of elements were obtained. In Appendix A, the Serpent results were compared to the experimental data by Walker et al. [22], where figures from these comparisons are shown and good agreement with the experimental data is evident.

As irradiated nuclear fuel is chemically very complex due to the presence of the tens of fission product elements, its exact modeling would be and is difficult. The complexity prohibits the use of detailed kinetic models with current methods, but the simplicity of thermodynamics allows its application even in this case. As Richard Feynman put it: “When knowledge is weak and the situation is complicated, thermodynamic relations are really the most powerful.” [24]

Even as thermodynamics allows us to use simple and powerful relations, simplifications are necessary to tackle the composition of nuclear fuel. The

Table 2.2. Grouping of elements occurring in nuclear fuel into representative elements in the order of ascending atomic number, as in Publication II. The elements calculated to occur by Serpent are shown, with the exception of B, N and C.

Representative element	Grouped elements
H	H
O	O
Y	Y
Zr	Zr, Nb
Mo	Mo, Zn, Pb, Fe, Co
Tc	Tc
Ru	Ru
Rh	Rh
Pd	Pd, Cd, Ag, Sn, In, Ge, Ga, Cu, Ni, Tl, Hg
Te	Te, Se, Sb, As, Bi, Po, At
I	I, Br
Xe	Xe, He, Kr, Rn
Cs	Cs, Rb, Li, Fr
Ba	Ba, Sr, Be, Ra
La	La, Tb, Dy, Ho, Er, Tm, Yb
Ce	Ce
Pr	Pr
Nd	Nd, Sm, Gd, Eu, Pm
U	U, Th, Pa, Ac
Pu	Pu, Am, Cm, Np, Cf, Bk

number of fission products appearing in nuclear fuel as calculated by Serpent is 72, including the initial uranium and oxygen, various fission products and the decay products of actinides. Thermodynamic data is not available for all of these elements, and some of the elements occur in minute amounts. It has become commonplace to group elements into representative elements according to chemical similarity (see, for example, [25, 26, 27] and Publication II), and use the mole amounts of the representative elements in calculations. In table 2.2 the grouping used in Publication II is shown for all elements calculated to occur in the fuel by Serpent except boron, nitrogen and carbon. These three elements are not included in the calculations due to lack of thermochemical data.

From initial investigations into the possible states of fission products in nuclear fuel, such as in [28, 29], the applications have grown in complexity over the years. In fission product transport and severe accident codes, thermochemical equilibrium analysis has found use already after initial applications [30, 31] to calculate the release behavior of fission products. It has also been included

Table 2.3. Commonly used thermodynamic potentials and their definitions in differential form [12].

Thermodynamic potential	Differential formula	Variables
Internal energy, U	$T\mathrm{d}S - p\,\mathrm{d}V + \sum_i \mu_i\,\mathrm{d}n_i$	S, V, n_i
Enthalpy, H	$T\mathrm{d}S + V\,\mathrm{d}p + \sum_i \mu_i\,\mathrm{d}n_i$	S, p, n_i
Helmholtz free energy, A	$-S\mathrm{d}T - p\,\mathrm{d}V + \sum_i \mu_i\,\mathrm{d}n_i$	T, V, n_i
Gibbs energy, G	$-S\mathrm{d}T + V\,\mathrm{d}p + \sum_i \mu_i\,\mathrm{d}n_i$	T, p, n_i

in mesoscale models of fuel behavior, such as the MFPR code [32]. Currently it is possible to couple the thermomechanical behavior of nuclear fuel and thermochemistry using the elemental composition determined by neutronics calculations. Such couplings are demonstrated in, for example, [33, 25, 27] and Publications I, II and III. Piro et al. [33] used a coupled thermomechanical, thermochemical and neutronic calculation to investigate the oxygen potential and chemical state of fission products in nuclear fuel, and Baurens et al. [25] used a similar approach to investigate corrosive gas release. This coupling has been further developed by Konarski et al. [27] to investigate oxygen thermodiffusion and its effect on corrosive gas release.

In this chapter and Publications I, II and III, development of computational methods for the study of nuclear fuel thermochemistry are presented. First, the basics of chemical thermodynamics and Gibbs energy minimization, the selected computational method, are presented. These methods are validated against experimental data regarding nuclear fuel in Publications I and II, and applied into practical issues regarding nuclear fuel in Publications II and III.

2.2 Determination of thermochemical equilibrium composition

2.2.1 Chemical equilibrium thermodynamics

In thermodynamics, the state of the system can be described with a thermodynamic potential, a measure of energy. Some common thermodynamic potentials are shown in table 2.3. The absolute values of the thermodynamic potentials are impossible to measure, but their changes are not. These changes lie at the core of practical chemical equilibrium thermodynamics.

From table 2.3 we observe that some of the potentials, namely internal energy and enthalpy, are functions of the entropy, a property that is very difficult to measure. On the other hand, the remaining two potentials, Helmholtz and Gibbs energies, are functions of temperature and volume or temperature and pressure, respectively. Temperature and pressure are intensive variables, that is, they are independent of the amount of matter in the system. In contrast, entropy and

volume are extensive variables, which do depend on the amount of matter.

Of these thermodynamic potentials, Gibbs energy is the only one dependent only on intensive variables, and extensive variables are held constant. In addition, it can be derived from the quantities in table 2.3 that the Gibbs energy is related to the enthalpy through the following relation:

$$G = H - TS, \tag{2.1}$$

and values of partial molar enthalpy are widely found tabulated. In practice, it is these partial molar quantities of thermodynamic potentials that are typically used. We define the partial molar quantity of any thermodynamic potential Z as

$$Z_i \equiv \frac{\partial Z}{\partial n_i}, \tag{2.2}$$

where all other variables that Z is dependent on are held constant. In addition, the extensive variable Z can be calculated from its constituent partial molar quantities as a linear combination as follows:

$$Z = \sum_i n_i Z_i. \tag{2.3}$$

If we integrate the differential representation of Gibbs energy from table 2.3, we find an important relation as the formulation reduces to

$$G = \sum_i \mu_i n_i, \tag{2.4}$$

where μ is the chemical potential, which is typically defined as the differential of Gibbs energy with respect to amount of matter,

$$\mu_i = \left(\frac{\partial G}{\partial n_i}\right)_{p,T,n_{j\neq i}} = G_i, \tag{2.5}$$

where G_i is the partial molar Gibbs energy.

For a pure species, its chemical potential can be defined as μ_i^p, with the partial molar enthalpy and the partial molar entropy:

$$\mu_i^p = H_i^p - TS_i^p \equiv G_f, \tag{2.6}$$

which also defines the Gibbs energy of formation of a species to be equal to the chemical potential of pure species. This is extremely convenient also for computational purposes. The superscript p for the chemical potential refers to the chemical potential of pure species, which is not equivalent to μ_i, the chemical potential of species i. The chemical potential of a pure species is only dependent on temperature, whereas the chemical potential of a species is also affected by other factors.

To calculate the chemical potential of a pure species, we must find the partial molar enthalpy and entropy at a given temperature for the pure species occurring in Eq. (2.6). These are typically tabulated for a standard temperature

and pressure state, and the temperature dependence is found from a isobaric heat capacity function. From this data, the partial molar quantities at any temperature are calculated as

$$H_i^p = H_{f,i}^\circ + \int_{T^\circ}^{T} C_{p,i} \mathrm{d}T + \sum_j \Delta H_{tr,i,j}, \tag{2.7}$$

$$S_i^p = S_i^\circ + \int_{T^\circ}^{T} \frac{C_{p,i}}{T} \mathrm{d}T + \sum_j \frac{\Delta S_{tr,i,j}}{T_{tr,i,j}}, \tag{2.8}$$

where S_i° is the standard entropy of the species and $H_{f,i}^\circ$ the enthalpy of formation of the species. $Z_{tr,i}$ are the entropy and enthalpy of phase transition, respectively, such as fusion or vaporization, and T_{tr} is the temperature of such a phase transition.

Chemically, any given system consists of a phase or phases, such as the gas phase or the solid phase. Gibbs [34] defined the phase as "a body with a distinct composition and thermodynamic state". The distinction between the solid phase and gas phase is quite obvious, but the distinction between mechanically inseparable solids with different crystal structures may not be. Gibbs [34] found a limit for the number of possible phases in any given system, called the Gibbs' phase rule. The phase rule is defined as follows:

$$P = C + 2 - F, \tag{2.9}$$

where P is the maximum number of phases that could be present in the system at equilibrium, C the number of independent components and F the degrees of freedom of the system. For a system dependent only on temperature, pressure and chemical composition, the phase rule reduces to the fact that the maximum number of phases present at equilibrium equals the number of independent components of the system. The independent components of a system are substances that may be used to form all species in the system as linear combinations from their molecular formulae. These components are not necessarily the elements, however, in the application to nuclear fuel, it is convenient to assume that the components equal the elements as the number of possible species in nuclear fuel is vast.

As Eq. (2.4) applies to each phase separately in the same manner as to the complete system, we may define the Gibbs energy of the complete system as the sum of the Gibbs energies of constituent phases as

$$G = \sum_{\phi=1}^{P} \sum_{i=1}^{S_\phi} n_i^\phi \mu_i^\phi. \tag{2.10}$$

Here P is the number of phases in the system, and S_ϕ the number of species in phase ϕ. The dependence of the chemical potential, μ_i, on temperature and pressure was already discussed previously, but in a system containing multiple

Table 2.4. Chemical potential functions for different types of substances.

Type of substance	Chemical potential expression
Pure gaseous species	$\mu^p + RT\ln p$
Pure condensed species	μ^p
Ideal gaseous species in a mixture	$\mu_i^p + RT\ln x_i p$
Ideal noncompressible condensed species in a mixture	$\mu^* + RT\ln x_i$
Nonideal gaseous species in a mixture	$\mu_i^p + RT\ln x_i\gamma_i p$
Nonideal noncompressible condensed species in a mixture	$\mu^* + RT\ln x_i\gamma_i$

species the chemical potential is also dependent on the chemical composition of the system. The derivations of the chemical composition dependences are derived in a number of sources, and the reader is referred to Ref. [35]. The relationships for some types of substances are shown in table 2.4. In the table, the pressure is dimensionless, with a reference state of 1 bar typically selected. In the expression for a condensed species (solid or liquid) in a mixture, the quantity μ^* is dependent on temperature, pressure and a standard compositional state, and defined by either the Raoult or Henry convention [35]. The quantity γ_i is the activity coefficient, containing the information on the nonideality of the mixture, and the term $RT\ln\gamma_i$ is often called the excess Gibbs energy, dependent on temperature, pressure and the chemical composition. The product of the activity coefficient and the mole fraction is the activity: $x_i\gamma_i = a_i$, a more fundamental quantity. The activity describes the "effective concentration" of the species.

2.2.2 Gibbs energy minimization

The equilibrium state of a system is the state of minimum energy. For chemical systems, the minimum of Gibbs energy is convenient to obtain due to the properties of Gibbs energy discussed in the previous section. At this minimum, the system has a certain composition, which is of interest to the modeller. This composition can be obtained by minimizing the Gibbs energy G in Eq. (2.10) and finding the associated mole amounts n_i for each species in the system. To obtain a reasonable solution, amount of matter in the calculation must be conserved. This is done by applying mass balance constraints, defined as

$$\sum_{i=1}^{S} a_{ij}n_i = b_j, \quad j = 1,...,C, \tag{2.11}$$

where S is the number of species in the system, a_{ij} are the stoichoimetric coefficients, C is the number of independent components in the system and b_j is the mole amount of component j. The stoichiometric coefficients are the multipliers used to form the composition of a species from the independent

components. A useful tool is the stoichiometric matrix **A**:

$$\mathbf{A} = \begin{bmatrix} a_{1,1} & a_{1,2} & \cdots & a_{1,C} \\ a_{2,1} & a_{2,2} & \cdots & a_{2,C} \\ \vdots & \vdots & \ddots & \vdots \\ a_{S,1} & a_{S,2} & \cdots & a_{S,C} \end{bmatrix}, \tag{2.12}$$

where the notation is as previously. This simplifies the mass balance constraints as

$$\mathbf{An} = \mathbf{b}, \tag{2.13}$$

where **n** is the mole amount vector and **b** the mass balance constraint vector.

There are a number of algorithms for this type of constrained minimization, Gibbs energy minimization (GEM). A general way to divide such algorithms is by classifying them with respect to the way mass balance constraints are used to find the minimum. Smith and Missen [35] divide the algorithms in this way to two groups: nonstoichiometric and the stoichiometric algorithms.

Stoichiometric algorithms use the stoichiometries of chemical reactions to eliminate the mass balance constraints completely. However, in this case, knowledge of the significant chemical reactions occurring in the system is required. Nuclear fuel contains a vast number of different chemical elements, and there is little knowledge on the reactions between each chemical constituent. Therefore, nonstoichiometric algorithms are better suited for the analysis of such systems. For the interested reader, Smith and Missen [35] describe both nonstoichiometric and stoichiometric algorithms, but here the discussion is limited to nonstoichiometric algorithms and one algorithm in particular.

A widely used nonstoichiometric algorithm is that of White [36], the RAND algorithm. Another similar algorithm is that of Brinkley [37, 35]. This class of algorithms is referred to by Smith and Missen [35] as the Brinkley-NASA-RAND algorithm, as another version was also developed at NASA. This type of algorithm was used in the multiphase system extension by Eriksson [38, 39, 40] in his SOLGASMIX program, which has since become famous. This algorithm has found wide use commercially, and a variation of the algorithm is implemented by the author in [12] and is used in Publications I, II and III.

The SOLGASMIX algorithm is a Lagrange multiplier method, where the constraints for the minimized equation are applied by the use of Lagrange coefficients. The multiphase equations are presented by Smith [41] and in useful matrix notation by Weber [42]. Often it is more convenient to use reduced quantities, divided by the factor RT and signified by a tilde. For example, for the chemical potential,

$$\tilde{\mu} = \frac{\mu}{RT}. \tag{2.14}$$

With reduced quantities, Eq. (2.10) becomes

$$\tilde{g} = \sum_{\phi=1}^{P} \sum_{i=1}^{S} n_i^{\phi} \tilde{\mu}_i^{\phi}, \tag{2.15}$$

and the minimization problem can be formulated as

$$\min \tilde{g} = \min \left(\sum_{\phi=1}^{P} \sum_{i=1}^{S} n_i^{\phi} \tilde{\mu}_i^{\phi} \right), \tag{2.16}$$

$$\text{subject to } \sum_{i=1}^{S} a_{ij} n_i = b_j, j = 1, ..., C,$$

$$\text{and} \qquad n_i \geq 0, i = 1, ..., S,$$

where the second constraint limits the mole amounts to positive values so that the solution has a physical meaning.

The derivation of the numerical equations by the Lagrange multiplier method is shown, for example, in [41, 35, 42, 12].

In a multiphase system, solving the Lagrange multipler problem for one assemblage of phases is not enough. To find out from a large collection of phases the phases yielding the minimum, successive collections of phases, here termed the phase assemblages, must be minimized. This iterative process is shown in figure 2.2, and it results in the local minimum. In this work, a separate global minimization routine has not been implemented.

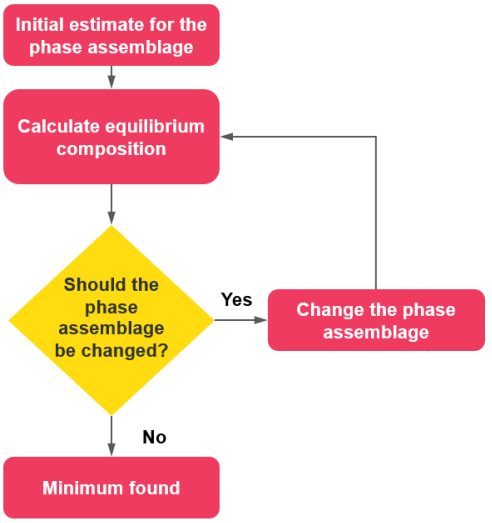

Figure 2.2. Minimizing the Gibbs energy of a multiphase system.

For each phase assemblage, the necessary and sufficient conditions for the minimum must be tested. The following equality must hold for all species present in the system [43, 44]:

$$\mu_i - \sum_{j=1}^{C} a_{ij} \Gamma_j = 0, \tag{2.17}$$

where Γ_j the Lagrange coefficient (chemical potential) of component j, and this equation is the necessary condition for the minimum. For each species not present in the system the following must hold:

$$\mu_i - \sum_{j=1}^{C} a_{ij}\Gamma_j > 0, \tag{2.18}$$

This is the sufficient condition for the minimum [43, 35].

In general, there are multiple rules that can be used to modify the phase assemblage. For example, a phase may be excluded from the calculation when its mole amount decreases to a sufficiently low value. In particular, a phase should be included in the local minimum calculation if Eq. (2.18) is violated with regards to the species. Several such rules must be used in order to obtain the minimum for the multiphase system.

2.2.3 Kinetically constrained equilibria

Only mass balance constraints were discussed in the previous section. However, it is also possible to limit the minimum with other constraints not based on conservation of mass, therefore called immaterial constraints. There are a number of constraints that could be used, and those are reviewed in detail by Koukkari [43] and Pajarre [45]. In Publication III, a kinetic constraint is used to perform a kinetically constrained equilibrium calculation on nuclear fuel. Koukkari et al. [46, 47] and Pajarre [45] describe methods of setting kinetic constraints. The constraint is applied in the minimization as an additional constraint b_j on the Gibbs energy equation. An additional column is required in the stoichiometric matrix as well. Effectively, the immaterial constraint forces the formation or decomposition of the species, if the stoichiometric coefficient of the immaterial constraint is nonzero for that species.

The value of the constraint b_j is determined in practice through an unconstrained equilibrium calculation and the kinetic model, which is used to obtain the extent of the reaction, ξ. The extent of reaction can then be used to constrain the equilibrium accordingly.

The extent of reaction relates the changes in mole amounts of reactants and products, and is expressed in moles. Suppose that a reaction

$$\nu_A A \leftrightarrow \nu_B B \tag{2.19}$$

proceeds towards the products so that dξ of A reacts. In this case the change in mole amount of A is dn$_A$ = -$\nu_A d\xi$, and for B dn$_B$ = $\nu_B d\xi$. Initially, ξ is defined to be 0. ξ is therefore related to the change in mole amounts by

$$d\xi = \frac{dn_i}{\nu_i}, \text{ and } \xi = \frac{\Delta n_i}{\nu_i}. \tag{2.20}$$

when expressed through the stoichiometric coefficient in the reaction, ν_i. In the application of Publication III, a kinetically constrained equilibrium under

irradiation is considered. We may define the equilibrium extent of reaction as ξ_{eq}, and a non-equilibrium value as ξ_{neq}. For the minimization,

$$b_{\mathrm{kin}} = \xi_{\mathrm{neq}}, \tag{2.21}$$

where b_{kin} is the value of the kinetic immaterial constraint.

2.3 Oxygen potential of nuclear fuel

Typical LWR nuclear fuel consists initially of uranium oxide, UO_2. When uranium undergoes fission, two fission product atoms are formed, but the amount of oxygen remains the same as it was initially. However, the fission products generally form species which contain less than two atoms of oxygen per fission, or even zero, such as the noble gases. Overall, fission is thought to free oxygen from the fuel. This in turn increases the oxygen potential of the fuel, which is defined as

$$\Delta G_{O_2} = \mu^p_{O_2} + RT \ln p_{O_2}. \tag{2.22}$$

However, values of oxygen potential are often reported with only the term dependent on the easily measurable partial pressure of oxygen, neglecting the standard chemical potential term $\mu^p_{O_2}$. In the following discussion, the oxygen chemical potential defined without the standard chemical potential is signified by quotation marks, so oxygen potential refers to the definition in Eq. (2.22) and "oxygen potential" to $RT \ln p_{O_2}$.

The oxygen potential of a substance is related closely to the composition of the substance. At equilibrium, a substance has a certain oxygen potential. The second term dependent on the partial pressure of oxygen can be measured. This measurement can yield information on the composition of the substance. With changes in the composition, the oxygen potential typically also changes. On the other hand, the oxygen potential can be changed by, for example, addition of oxygen, and with time the composition of the substance changes to reflect the new oxygen potential, in essence by reacting with oxygen.

The exact chemical composition is difficult to measure from nuclear fuel, whereas "oxygen potential" – when defined without the standard chemical potential of oxygen – can be measured with less difficulty. Therefore this definition of oxygen potential is a useful proxy for the chemical composition, which is of interest, and the oxygen content of the fuel in itself has effects on the performance of fuel: it has been shown that oxygen released from the pellet may prevent crack formation in the cladding [15] and influence the release of corrosive gases from the pellet [27].

The Gibbs energy minimizer developed initially in [12] is validated and verified further with several experimental data sets regarding "oxygen potential" in Publication II. For example, the calculated "oxygen potential" of pure uranium oxide is compared to experimental data at 1273 K in figure 2.3, showing good agreement. On the other hand, the irradiated results were verified with

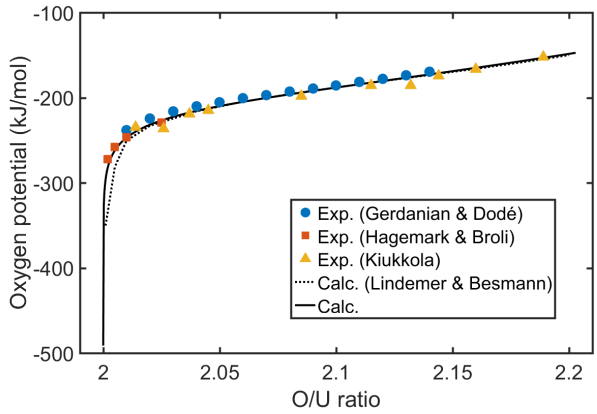

Figure 2.3. The calculated "oxygen potential" of UO_2 compared to experimental data from Gerdanian and Dodé [48], Hagemark and Broli [49] and Kiukkola [50]. In addition, values calculated with the Lindemer-Besmann model [51] are shown. For the purposes of this figure, the "oxygen potential" is defined as $RT\ln p_{O_2}$, without the standard chemical potential term (see Eq. (2.22)). Figure reproduced from Publication II.

reference calculations from [44] in figure 2.4, where the "oxygen potential" of a hypothetical mixture of fission products (U, Pu, Ru, Ba, Sr, La, Mo, Cs and Zr) and actinides was calculated with different initial amounts of oxygen. The differences between the two results are most likely due to simplifications made in this work, for example the treatment of noble metal phases as ideal. Finally, in figure 2.5, the "oxygen potentials" calculated in Publication II are compared to experimental data from Walker et al. [22], showing good agreement. In all the cases where the experimental and calculated values of "oxygen potential" are compared, the "oxygen potential" is defined as $RT\ln p_{O_2}$, without the standard chemical potential term (see Eq. (2.22)).

An interesting feature is evident from the experimental results in figure 2.5. The oxygen-to-metal ratio reported by Walker et al. [22] was 2.005, and the "oxygen potential" of urania with this oxygen stoichiometry is shown in the figure with a dashed line. From this it is evident that the "oxygen potential" would have decreased from its initial value. This is also the result obtained from the calculations. If the fuel was exactly stoichiometric UO_2, then the expected increase would be present in the data.

In Publication I, the "oxygen potential" evolution with burnup is calculated with various initial oxygen-to-metal ratios both in the hypo- and hyperstoichiometric domains. The main results of these calculations are shown in figure 2.6. In these investigations, the thermochemical modeling shows that for hyperstoichiometric fuel the "oxygen potential" drops with burnup, whereas with stoichiometric or hypostoichiometric fuel the "oxygen potential" increases with burnup. However, in the hyperstoichiometric domain only the initial oxygen-to-metal ratios close to the stoichiometric composition show this effect, and at higher oxygen-to-metal ratios the "oxygen potential" does not show a similar

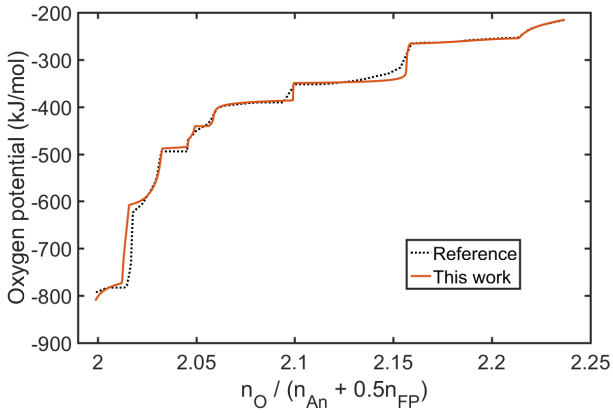

Figure 2.4. Comparison of the calculated "oxygen potentials" at 1.0123 bar and 1023 K to oxygen potential results presented in [52]. For the purposes of this figure, the "oxygen potential" is defined as $RT\ln p_{O_2}$, without the standard chemical potential term (see Eq. (2.22)). In the x-axis title, n_i refers to mole amount of i, An to actinides and FP to fission products. Figure reproduced from Publication II.

sharp drop.

A different rod and a different burnup calculation is investigated in Publications I and II, but a similar effect can be seen in Publication II, as shown in figure 2.7. In this figure, the buffering effect of the $UMoO_6$ compound is also shown. This buffering effect would effectively keep the "oxygen potential" constant with burnup. However, studies [20] have shown that this coumpound would not form in nuclear fuel. The "oxygen potentials" depicted by dashed lines shown in figure 2.7 can therefore be said to be closer to reality.

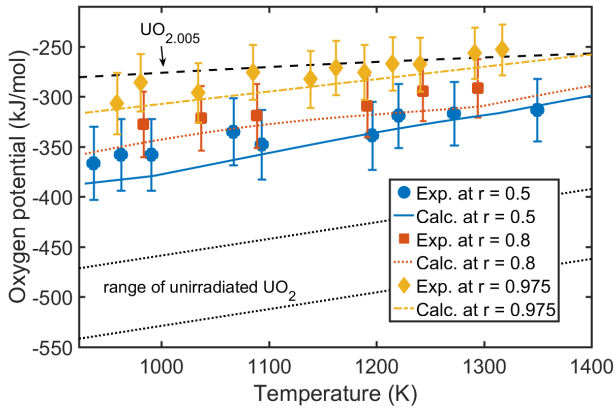

Figure 2.5. Comparison of calculated "oxygen potentials" with the experimental results of Walker et al. Fresh fuel is represented by the black dashed line for $UO_{2.005}$. For the purposes of this figure, the "oxygen potential" is defined as $RT \ln p_{O_2}$, without the standard chemical potential term (see Eq. (2.22)). Figure reproduced from Publication II.

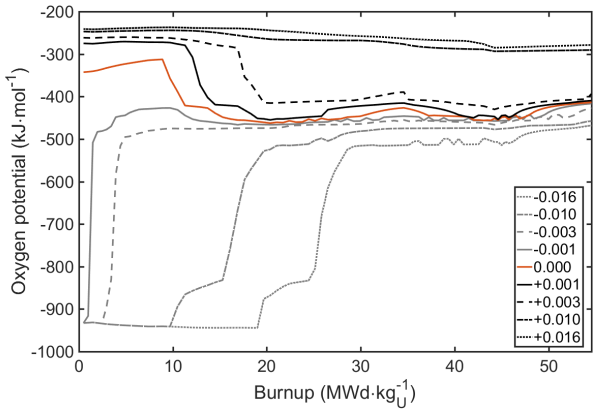

Figure 2.6. Variation of "oxygen potential" with burnup for several different initial oxygen-to-metal ratios. Figure reproduced from Publication I. For the purposes of this figure, the "oxygen potential" is defined as $RT \ln p_{O_2}$, without the standard chemical potential term (see Eq. (2.22)).

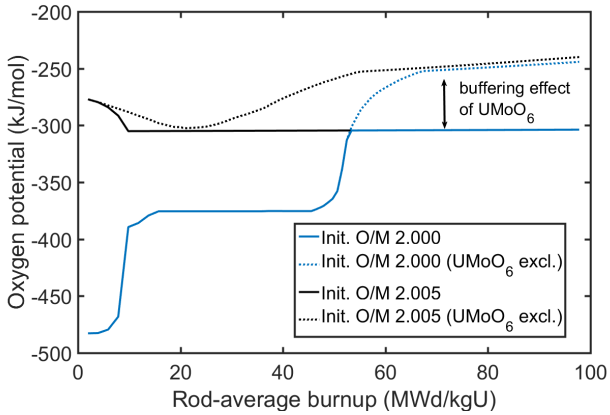

Figure 2.7. Variation of "oxygen potential" with burnup for two different initial oxygen-to-metal ratios, and the supposed buffering effect of the $UMoO_6$ species. For the purposes of this figure, the "oxygen potential" is defined as $RT \ln p_{O_2}$, without the standard chemical potential term (see Eq. (2.22)). Figure reproduced from Publication II.

2.4 Cesium iodide radiolysis

Iodine is thought to be a corrosive agent involved in stress corrosion cracking of nuclear fuel cladding. Stress corrosion cracking is often thought to cause failures of the cladding through pellet-cladding interaction (PCI) [53, 54, 55]. Failure of the cladding through PCI requires both sufficiently high mechanical stress on the cladding as well as the presence of a corrosive substance. The failure of the cladding leads to the loss of a release barrier of radioactive nuclides and these materials may then contaminate the primary coolant circuit. Defective fuel rods must be removed from the core, which may cause financial losses in terms of unplanned shutdowns and also increase radiation doses of the plant personnel due to contamination of the primary circuit. Various remedies have been developed for PCI, including coatings for the cladding interior and power ramp rate limits, for example, but there still is a significant interest to develop more effective PCI mitigation strategies [55].

Understanding the behavior of iodine in nuclear fuel is very important in the effort to prevent the PCI phenomenon. The most common theory on what causes the corrosive effect iodine has on the cladding is the van Arkel and de Boer process, in which iodine species react with zirconium in the cladding forming gaseous zirconium tetraiodide, ZrI_4, and this causes cracks to propagate [54, 55]. Some important elements that may react with iodine are among the fission products formed in nuclear fuel. These are mainly the alkali and earth alkali metals: cesium, rubidium, strontium and barium. These metals form iodides which are inert regarding the reaction with zirconium to form ZrI_4, but atomic and molecular iodine – I and I_2 – are reactive towards zirconium. Quite recently attention was placed on the appearance and reactivity of TeI_2 [56, 25]. Hydrogen also forms in small amounts in the fuel, and hydrogen iodide, if formed, would be reactive. Hydrogen formation through nuclear reactions has not been taken into account in fuel thermochemical calculations in the literature, and hydrogen may also be present as an impurity from residual moisture in the pellet remaining from the manufacturing process.

Most iodides have relatively low melting points, with the one thought to be most abundant, cesium iodide, melting at around 900 K. However, even such temperatures are not achieved in light-water reactor fuel pellet-cladding gap outside of accidental conditions. During normal operation of the fuel, cesium iodide would occur as a solid, and have a low vapor pressure. Though these iodides do not react with zirconium, there is an intense radiation field in the fuel-cladding gap that may decompose these iodides into the corresponding metal and free iodine through radiolysis. This iodine would then be available for reaction with the cladding.

Konashi et al. [57, 58] have modelled the radiolysis of cesium iodide in the gas phase extensively, and this is the basis of much of the work in Publication III. In addition to Konashi et al., several other authors have also modeled cesium iodide radiolysis. For example, Ball et al. [59] calculated the effect of fission fragments

on cesium iodide and cesium telluride in the gas phase. Filin et al. [60] included oxygen-containing species in their kinetic calculations, and Lewis et al. [61] calculated solid cesium iodide radiolysis with a simple model which assumes that fission fragment energy deposits in a solid layer on the fuel pellet surface and causes the cesium iodide to dissociate. In Publication III, the latter type of model is applied along with a gas phase radiolysis model, which allows for the evaluation of their combined effect.

The reactions considered in detail in this model were as follows:

$$\mathrm{Cs} + \mathrm{I} \underset{k_{d1}}{\overset{k_{r1}}{\rightleftharpoons}} \mathrm{CsI} \tag{2.23}$$

$$2\mathrm{I} \underset{k_{d2}}{\overset{k_{r2}}{\rightleftharpoons}} \mathrm{I_2} \tag{2.24}$$

$$\mathrm{Cs} + \mathrm{I_2} \underset{k_{d3}}{\overset{k_{r3}}{\rightleftharpoons}} \mathrm{CsI} + \mathrm{I} \tag{2.25}$$

$$\mathrm{CsI} \underset{k_{d4}}{\rightarrow} \mathrm{Cs} + \mathrm{I} \tag{2.26}$$

The fourth reaction is the dissociation reaction due to radiolysis. The reaction rates for these reactions have been reported by Konashi et al. [57], with k_{d4} consisting of rates due to two processes, radiolysis caused by fission fragments and the collision cascade due to fission fragments. The reaction rates for Eqs. (2.23) through (2.25) are taken as is from Konashi et al. [57], but the calculation of the components of k_{d4} is revisited. In addition, the previous reactions apply in the gas phase, but we must define two other reactions for the transfer of cesium iodide into and from the solid phase:

$$\mathrm{CsI\ (s)} \underset{k_{d5}}{\overset{k_{r6}}{\rightleftharpoons}} \mathrm{CsI\ (g)}, \tag{2.27}$$

The forward reaction describes the vaporization of cesium iodide, whereas the backward reaction describes the condensation of cesium iodide onto the fuel surface.

Konashi et al. [57] calculate the reaction rate constant k_{d4} with collision theory, assuming

$$k = \int_0^{E_0} \phi \sigma dE, \tag{2.28}$$

where ϕ is the flux of the energetic particles, σ the dissociation cross section of cesium iodide, E the kinetic energy and E_0 the initial (maximum) kinetic energy of the energetic particles. Both ϕ and σ are dependent on the kinetic energy. Collision theory is the approach adopted also in Publication III.

The main difference in this work, in addition to the inclusion of dissociation of solid cesium iodide, is the fission fragment flux. Konashi et al. use the fission fragment flux derived by Olander [1] for use fission gas bubble resolution, where the used flat energy distribution applies to the fragments inside the fuel grain:

$$\phi_{\mathrm{ff}} = \dot{F} R_{ff} f_E = \frac{\dot{F} R_{ff}}{2E_0}. \tag{2.29}$$

However, the energy distribution of fission fragments that reach the fuel (pellet) surface is quite different. This distribution can be derived from geometric considerations to be [62] (see the derivation in Appendix B):

$$f_E = \frac{1}{8E_0}\left(\frac{E}{E_0}\right)^{-\frac{1}{2}}. \tag{2.30}$$

The above distribution results in that most fission fragments have a very low energy. The low energy fission fragments have been shown by Konashi et al. [63] to be most significant in the radiolysis of cesium iodide.

The gas phase kinetic model was first verified against the work of Konashi et al. The updated model produced thousand-fold differences in the gas concentrations of atomic and molecular iodine. The difference was caused mostly because of the revised dissociation rate constants based on the updated fission fragment flux. However, an even larger difference was found in that Konashi et al. [57] assumed the equilibrium concentrations of iodine species to be much lower than those of cesium and cesium iodide based on a simple thermochemical analysis. A detailed thermochemical equilibrium calculation on fuel reveals that the equilibrium concentrations of atomic and molecular iodine may be much higher, and only an order of magnitude smaller than that of cesium iodide. The effect of radiolysis in this case would be negligible.

Due to this finding, the solid cesium iodide vaporization and condensation was taken into account in the model. Due to the initially low partial pressure of cesium iodide at the pellet-cladding gap, this equilibrium reaction was selected to be analyzed with a kinetic constraint in Gibbs energy minimization. The mole amount of solid cesium iodide corresponding to the extent of reaction ξ_{irr} in Eq. (2.21) can be calculated from the results of the kinetic model and used as an immaterial constraint in the Gibbs energy minimization. This way the thermodynamically most stable species that would form from the cesium and iodine freed by radiolysis is determined in Publication III.

Hydrogen iodide seems to be a more thermodynamically favourable form of iodine than cesium iodide at low temperatures. Its reaction with zirconium is also favourable, so it can therefore be possible that also hydrogen iodide plays a role in iodine stress corrosion cracking. As a real fuel surface does not reach thermochemical equilibrium due to its low temperature and transient effects of temperature and composition change, results calculated by such a method are prone to large uncertainties. However, useful qualitative information can be obtained by such an endeavor.

3. Nuclear fuel thermomechanics

3.1 Background

The overall behavior of the nuclear fuel rod must be known so that the integrity of the cladding, the first release barrier of radioactivity, is ensured. As experiments on irradiated fuel are expensive and time-consuming, well-validated computational tools are necessary for the investigation of the effect of different operational regimes on the behavior of nuclear fuel. In addition, instrumented experiments cannot be performed in power reactors, where there is no space for instrumentation. The experiments in research reactors have to emulate the conditions in a power reactor, never being exactly similar to real conditions, so extrapolation to real conditions is always necessary. The tools validated with this kind of experimental data can then be used to show compliance with various regulatory criteria, for example.

Nuclear safety is regulated both domestically by the national authority but also internationally by the International Atomic Energy Agency (IAEA). The guidelines set forth by the IAEA are more general than the requirements by the national authority. In the case of fuel, for example, the IAEA Safety Guide NS-G-1.12 [64] sets various requirements for fuel design and performance. However, in this discussion, the focus is on the Finnish regulations. The Finnish Radiation and Nuclear Safety Authority (STUK) has decreed [65] as follows:

> The safety of a nuclear facility shall be assessed when applying for a construction license and operating license, in connection with plant modifications, and at Periodic Safety Reviews during the operation of the plant. It shall be demonstrated in connection with the safety assessment that the nuclear facility has been designed and implemented in a manner that meets the safety requirements. The safety assessment shall cover the operational states and accidents of the plant. The safety of a nuclear facility shall also be assessed after accidents and, whenever necessary, on the basis of the safety research results. The nuclear facility's safety and the technical solutions of its safety systems shall be assessed and substantiated analytically and, if necessary,

experimentally.

The analytical tools, referred to in the decree, used to substantiate the safety of nuclear power plants can be roughly divided into deterministic analyses and probabilistic risk assessment methods. The analysis of nuclear fuel falls into the former class. The models used to predict nuclear fuel behavior given certain boundary conditions are deterministic, that is, given a certain initial state and boundary conditions, the predictions are the same regardless of how many times the model is run.

There are a number of conditions of the nuclear power plant for which these safety analyses must be performed. Firstly, the normal operation of the power plant must be analyzed. Normal operation refers to operation of the plant in a planned way, including testing, plant start-up and shutdown, maintenance and fuel replacement [65]. Secondly, deviations from normal operation must be analyzed and nuclear safety ensured in these cases. Deviations from normal operation are classified into several types based on the frequency of their occurrence. The most common type of deviation, with a frequency of one or more times in a hundred operating years, is the anticipated operational occurrence [65]. Less common deviations are termed postulated accidents, which are assumed to occur less frequently than once in one hundred operating years [65]. STUK presents detailed regulatory requirements in the Regulatory Guides on nuclear safety, in short called the YVL guides, of which the guide B.4 [66] relates to nuclear fuel. According to the guide, for example, in normal operation, the fuel is not allowed to melt, the rod internal pressure is not allowed to increase excessively and in anticipated operational occurrences the possibility of fuel failures caused by mechanical interaction between the pellet and the cladding must be minimal.

Parameters such as fuel temperatures, rod internal pressure or cladding stresses and strains can be analyzed with dedicated fuel performance codes, and so the safe operation of fuel can be ensured. Many different fuel performance codes are developed around the world. Several are currently in use at VTT: U.S. Nuclear Regulatory Commission (US NRC) has developed the FRAPCON [67] and FRAPTRAN [68] fuel performance codes, designed for the analysis of steady-state and transient fuel behavior, respectively. The ENIGMA [9] fuel performance code was originally developed by Nuclear Electric in the United Kingdom, and development of a branch of this code has continued at VTT over the years [10]. The SCANAIR code in turn is designed for reactivity insertion accident simulations and developed by IRSN in France [69]. Traditional fuel performance codes have focused on the most widespread cylindrical geometry with ceramic actinide oxide pellets and metallic cladding, and several simplifications can be made in these codes due to the simple geometry. Quite recently, Idaho National Laboratory has developed the BISON fuel performance code [70] for three-dimensional finite-element analysis of nuclear fuel, which allows for more detailed analysis of traditional fuels but also the analysis of more exotic

geometries planned for future fuel types.

The FINIX fuel behavior module has been under development at VTT since 2012. The purpose of FINIX is to develop an easy-to-use fuel behavior interface for multiphysics applications, where several solvers dealing with certain physical phenomena are coupled together for a more accurate description of reactor core behavior. Publications IV and V describe further development of FINIX, and the main results from this stage of development are summarized in the next sections.

Fuel performance codes typically describe material properties of fuel rod components with empirical correlations fitted to data. Material properties such as thermal conductivity and expansion or elastic modulus and yield strength are obtained from these correlations and used to solve the thermal and mechanical behavior of the fuel rod. The thermal and mechanical behavior must be solved simultaneously due to their interconnected nature. The pellet-cladding gap width is an especially interconnected parameter, as the gap is the least thermally conductive part in the radial direction. Several phenomena affect the gap width: differences in thermal expansions of the pellet and cladding, swelling of the pellet due to accumulation fission products, creepdown of the cladding in the higher coolant pressure relative to the rod internal pressure and so on.

As the fuel rod is very long, typically several meters, compared to its diameter, typically roughly one centimeter, the axial variations in a single location can be assumed to be quite small. Therefore the typical assumption in fuel performance codes is to separate the rod into several axial sections, solving the behavior along the fuel rod radius in one dimension independently of the neighbouring axial sections [71]. However, it is typically assumed that the internal pressure of the fuel rod is identical in all sections. This is termed the 1.5-dimensional approach, which is typical of many fuel performance codes [71].

The validity of the predictions of fuel performance codes is of course very important, and can only be proven by comprehensive validation efforts. Due to the interconnected nature of fuel behavior phenomena, one typical way is to perform integral validation by comparing some measured parameters from integral fuel rod experiments to predicted ones. In such experiments, an instrumented fuel rod is irradiated in an experimental reactor, and the instruments record the temperature, pressure or deformation of the fuel rod. The OECD/NEA Halden Reactor Project provided ample amounts of such data until the closure of the Halden reactor in Norway in 2018. FINIX has also been validated against several experiments performed at Halden, and these results are shown in the coming sections. Another method is validating the code with separate effects experiments, where a single physical phenomena is investigated with an experiment instead of the behavior of the fuel rod as a whole. In the following, such experiments, again from the Halden reactor, are also used in the validation of FINIX.

3.2 The fuel behavior module FINIX

Fuel behavior models in other codes, such as thermal hydraulics and neutronics codes, are often very simple. They may be based on simple correlations, non-mechanical thermal elements or fixed values of temperature. Such models may not be realistic in transient conditions or at extended burnup, and these cases are very typical, not the exception. The purpose of FINIX is to provide a better fuel behavior description for such codes while remaining sufficiently simple to use. The source-code level interface of FINIX has been designed so that its coupling with other solvers is simple, with a high-level syntax and convenient error processing mechanisms. The FINIX approach was first described in detail in Publication IV. Ideologically similar approaches have been taken, for example, in the DYN3D code with its internal fuel model [72], in the simplified version of FRAPTRAN used with MARS-KS system code [73] or in the simplified fuel model in SIMULATE5 nodal neutronics code [74].

The initial versions of FINIX contained only basic thermomechanical simulation capabilities, solving the elastic mechanical equations and the heat equation. From the first validation of FINIX, described in [8] and Publication IV, the performance of FINIX can be seen to be good in transient conditions. However, with increasing burnup in simulations of long irradiations, the accuracy of, for example, the temperature predictions was not sufficient. Since then, several directly or indirectly burnup-dependent models are implemented in FINIX as shown in Publication V. The main features of these models are briefly introduced in the next section.

The solution method used in FINIX to obtain the fuel rod temperatures and deformations is typical of fuel performance codes, and is shown in figure 3.1. The solution proceeds in discrete time steps, and on each time step the thermal and mechanical solutions are found by numerical iteration. The method can be divided into two main loops: the outer loop finds the thermal solution, within which the inner mechanical loop solves the internal pressure and pellet and cladding deformations. Two different solvers can be used in finding the thermal solution depending on the calculated scenario; for large time steps the steady-state solver is appropriate whereas for fast transients the transient solver should be used.

The most central part of FINIX is the one-dimensional cylindrical heat equation,

$$C_v \frac{\partial T}{\partial t} - \frac{1}{r}\frac{\partial}{\partial r}\left[\lambda r \frac{\partial T}{\partial r}\right] - s(r) = 0. \tag{3.1}$$

where C_v is the isochoric heat capacity, dependent on temperature, T the temperature, λ the thermal conductivity, dependent on temperature, and s the heat source. The solution is obtained by discretizing the heat equation in space and solving the resulting equations at each time step. For the pellet and cladding, the changes in their density over time through thermal expansion or other processes such as swelling due to fission product accumulation changes the radial locations

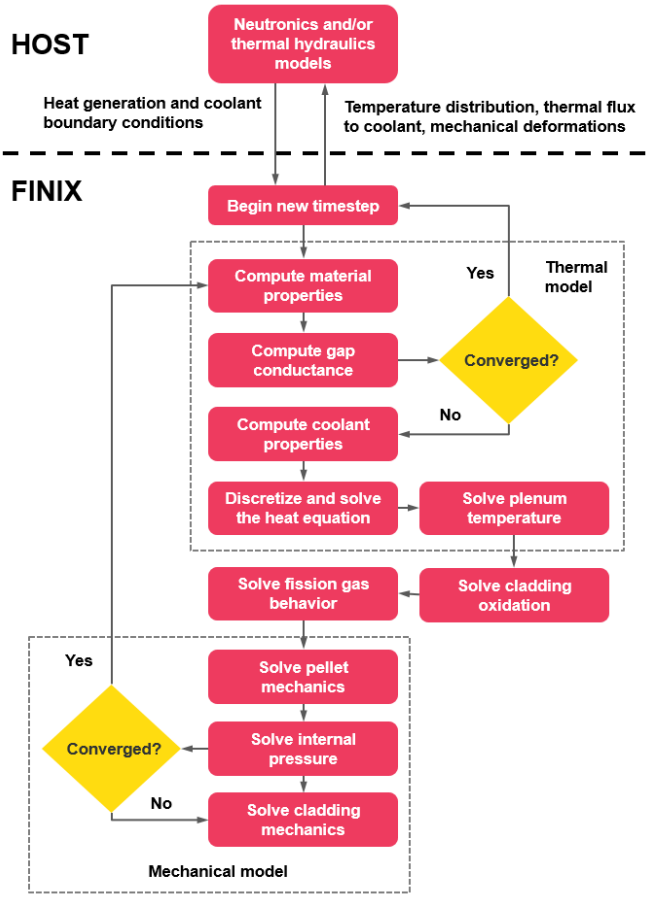

Figure 3.1. The FINIX iteration scheme. Figure reproduced from Publication V.

r_i, which in turn affect the thermal solution. An especially important boundary condition in this type of fuel is that between the fuel pellet and the cladding:

$$q(R_f) = -\lambda(T(r))\frac{\partial T}{\partial r}\bigg|_{r=r_f} = h\left[T(r_f) - T(r_{ci})\right], \tag{3.2}$$

where λ is the thermal conductivity of the material and h the heat transfer coefficient of the gas gap between the pellet and the cladding. The heat transfer coefficient h given as a sum of three terms:

$$h = h_{\text{cond}} + h_{\text{rad}} + h_{\text{contact}}, \tag{3.3}$$

where h_{cond} refers to conduction heat transfer coefficient, h_{rad} to radiative heat transfer coefficient and h_{contact} to contact heat transfer coefficient. These are heavily dependent on the width of the gas gap, which connects the thermal and

mechanical solutions. For example, the conduction heat transfer coefficient is defined as

$$h_{\text{cond}} = \frac{\lambda_g}{l}, \tag{3.4}$$

where λ_g is the thermal conductivity of the gas gap and l a characteristic length. In this case, the characteristic length is the width of the gas gap, and as it increases, the conduction heat transfer coefficient decreases.

The pellet in FINIX is treated as an undeformable solid, often called the rigid pellet approximation. The cladding mechanics are, on the other hand, more complex. In the calculation of stresses in a cylinder, the cylinder can be treated either as a thick-walled or a thin-walled cylinder. In a thick-walled cylinder, the stresses within the cylinder wall are nonuniform. For example, in a thick-walled cylinder, the hoop stress σ_θ at radius r is defined as

$$\sigma_\theta(r) = \frac{r_{ci}^2 p}{r_{co}^2 - r_{ci}^2}\left(1 + \frac{r_{co}^2}{r^2}\right) \tag{3.5}$$

where r_{ci} is the inner radius and r_{co} the outer radius of the cylinder wall, and p the pressure difference over the cylinder wall[1]. In the thin-walled approximation, the expression is much simpler:

$$\sigma_\theta = \frac{p r_m}{r_{co} - r_{ci}}, \tag{3.6}$$

where $r_m = \frac{r_{ci}+r_{co}}{2}$ is the midplane radius of the cylinder wall. A thin-walled assumption is valid when the ratio of cylinder inner radius to cylinder wall thickness is sufficiently large. Ratios ranging from 5 to 20 can be found from the literature as the limit, and 10 seems to be the most common value. A thin-walled assumption is typically made in fuel performance codes[9, 67, 68], even though with typical values of 0.6 mm wall thickness and 4.5 mm cladding inner radius the ratio is only 7.5. In FINIX the assumption has been made to simplify the code, and as such its use is justified, but for a high-fidelity description of cladding stresses, the thick-walled assumption should be used.

In addition to these relationships, the strains in the cladding must be related to the stress. In FINIX, Hooke's law in cylindrical coordinates is used, and for example the hoop strain is defined as

$$\epsilon_\theta = \frac{1}{E}(\sigma_\theta - \nu\sigma_z) + \sum_i^{\text{th,pl,c}} \epsilon_\theta^i \tag{3.7}$$

where E is the elastic modulus, ν the Poisson's ratio and ϵ^i different components of strain such as thermal (th), time-independent plastic (pl) or creep (c). In Publication V, the implementation of the models for the calculation of time-independent plastic and creep strains are shown. More detailed descriptions than permitted by a journal article are found from the FINIX user's manuals, the latest of which is that of version 1.19.1 [5].

[1]Assuming the radial stress σ_r at r_{ci} equals $-p_i$ and at r_{co} it equals zero.

3.3 Implementation of burnup effects in FINIX

3.3.1 Pellet swelling

The evolution of pellet composition with burnup as fission products form in the pellet changes also the molar volume of the pellet and therefore its dimensions. In this respect, the fission products can be divided into two classes: the gaseous and the solid fission products.

Regarding solid fission products, Olander [1] related the change in fuel pellet volume into the difference in molar volumes of the initial uranium oxide and the resulting chemical forms of the fission products. Olander derived the following relation:

$$\frac{\Delta V}{V} = \left(\sum_i \frac{Y_i V_{m,i}}{V_{m,UO_2}} - 1 \right) B, \tag{3.8}$$

where Y_i is the fission yield of fission product i, $V_{m,i}$ the molar volume of i and B the burnup. For example, Anselin [75] calculated the term in brackets assuming plausible chemical states for each fission product and using the fission yields of a certain fissile nuclide. Because fission yields for different fissile nuclides are different, the term must be calculated for each fuel separately.

The term in brackets is approximately constant while the fissioning nuclide stays the same. However, that is not the case in nuclear fuel, as with irradiation, fissile higher actinides form. For example, in fuel with ^{235}U as the fissile nuclide, the fissions occur initially in ^{235}U. After a certain period of time, sufficient ^{239}Pu will have been formed for it to contribute considerably, which also changes the fission yields of fission products.

In FINIX, a correlation from FRAPCON [67] is implemented (see Publication V), where the swelling strain is linearly dependent on the burnup. The burnup is given in units of MWd·kg$_U^{-1}$ and its multiplier is simply $6.2 \cdot 10^{-4}$ between burnups of 6 to 80 MWd·kg$_U^{-1}$ and $8.6 \cdot 10^{-4}$ above 80 MWd·kg$_U^{-1}$.

The effect of gaseous fission products is more complex than that of the solid fission products. The models in fuel performance codes taking into account this effect range from the more mechanistic [76] related closely to modeling the fission gas release from the pellet to more simplistic [67] such as the model in FRAPCON. In Publication V, a simple model from FRAPCON is implemented in FINIX.

3.3.2 Pellet densification

From fabrication a fuel pellet is always porous to some extent, typically in the order of 95 % of theoretical density. This porosity in part balances the effect of swelling, as the swelling decreases the porosity. In the start of reactor operation, another process called densification changes the dimensions of the fuel pellet by reducing the porosity.

Out of reactor, sintering is a similar process occurring when a material is held at a high temperature. Sintering occurs as the free energy is decreased by decreasing the surface area of the grains of the material. However, the thermal energy is not enough to cause such sintering in typical irradiation of nuclear fuel due to relatively low temperatures. Under irradiation, athermal sintering is possible [77], which is based on vacancy diffusion [77, 1]. This process is called densification.

Densification has an effect in the very beginning of irradiation, decreasing the pellet radius. Later in the irradiation swelling has a more significant effect, causing the increase in pellet radius.

A model from MATPRO[78]/FRAPCON[67] was implemented in FINIX to describe fuel densification. In densification models, typically a measured resintering density change is used to tune the densification model for each simulated case. A resintering test where a fuel pellet is sintered at 1700 °C for 24 hours is typical [79], and the measured densification from this test is used as a tuning parameter. However, to simplify FINIX input, the tuning parameter – resintering density change – is assumed to have a value of 100.0 $kg \cdot m^{-3}$ by default.

3.3.3 Radial power distribution

Fission density in nuclear fuel is not evenly distributed across the pellet, but is higher at the fuel surface. This is because of high cross sections for capture and fission in the fuel and so neutrons interact with the fuel most on the pellet surface. The power density is of course proportional to the fission density, and the fission density is proportional to the number of fissionable nuclides. In figure 3.2, the plutonium concentration across the pellet radius is shown, and the radial power distribution has a similar shape.

Apart from steady-state irradiation behavior, where the radial power distribution causes an uneven burnup distribution in the pellet, the radial power distribution is important in transients. For example, in a reactivity insertion accident, the highest volumetric heat generation rate occurs at the pellet surface. This causes a peculiar behavior during the transient where the temperature rises on the pellet surface fastest, and only later diffuses to the central part of the pellet and stabilizes to the steady-state parabolic temperature distribution. This behavior is illustrated in figure 3.3, where the radial temperature profile is shown for a RIA up to 20 milliseconds from the power pulse. In this particular RIA, the power begins to rise at 0 ms and reaches its peak at 3 ms. Even though in applications where FINIX is coupled to a neutronics solver the power distribution along the pellet radius is obtained from the other solver, this is not the case when FINIX is coupled to, for example, a thermal hydraulics solver. Due to the importance of the radial power distribution in these cases, especially in transient simulations, the implementation of a separate model within FINIX was worthwhile.

In FINIX, the TRANSURANUS Burnup Equations (TUBRNP) model [80]

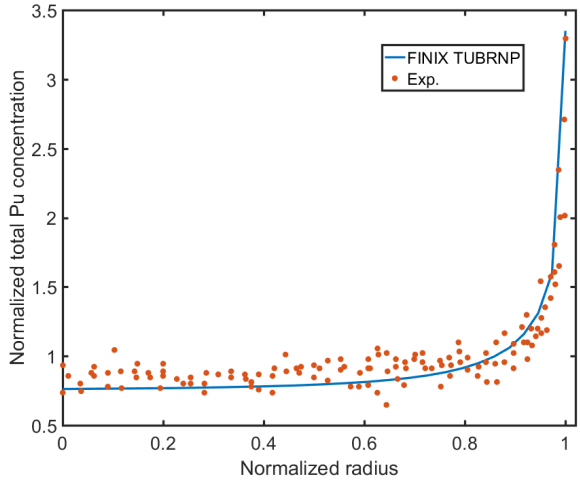

Figure 3.2. Plutonium concentration as calculated by the FINIX implementation of the TUBRNP radial power distribution model compared to experimental data. Figure reproduced from Publication V.

is implemented and described in part in Publication V. The TUBRNP model tracks the amounts of actinide nuclides and through their amounts derives the radial power distribution within the fuel. There are multiple versions of the TUBRNP model, and the version implemented in FINIX is the most simple containing only uranium isotopes ^{235}U and ^{238}U as well as plutonium isotopes with mass numbers ranging from 239 to 242. In particular, this version does not include support for the presence of burnable poisons such as gadolinium, so gadolinia-doped fuel cannot be modeled correctly with the standalone FINIX.

3.3.4 Fission gas release

Approximately one third of fission products of ^{235}U are noble gases, mostly xenon and krypton. The appearance of additional gas within the fuel rod increases the internal pressure of the rod. However, as the fission products appear within the fuel grains where fissions occur, they must first transport out of these grains to the grain boundaries and finally to the free volume within the rod. In table 3.1 the most important processes typically modeled by fission gas release models are shown. In the following, each process and the modeling approaches taken in FINIX are discussed in the same order.

Gas production in fuel is of course related to the fission rate within the fuel, which in turn is related to the power density. In FINIX, a simple linear correlation is established between the power density and fission rate, as per Massih and Forsberg [82], which yields the source term of fission gas atoms for the release model.

Blair [81] notes that for stable gas atoms, recoil and knockout as release

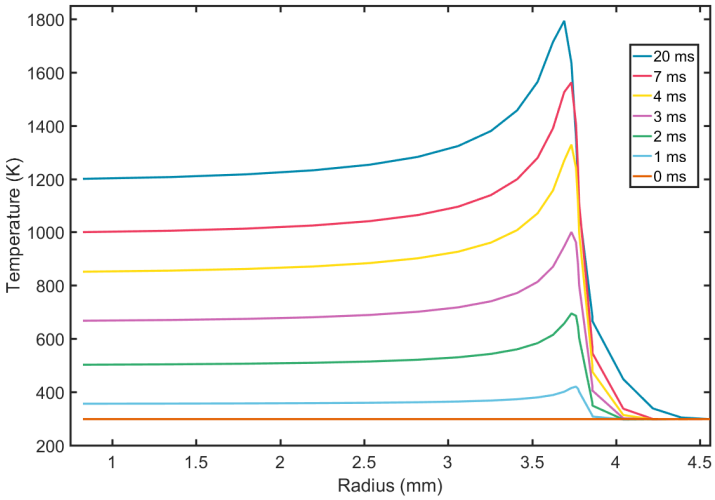

Figure 3.3. Rod temperature distribution of a fuel rod in a reactivity insertion accident during the first 20 milliseconds as calculated by FINIX. Power pulse peak occurs at 3 ms, and the gas gap is located at 3.8 mm. The shape of the temperature profile is determined by the radial power distribution.

processes are insignificant compared to other processes. For unstable gas atoms, these processes are important, however, but the current FINIX model focuses on the release of stable gas atoms in steady-state conditions.

The first phenomena to solve in fission gas release is that of intragranular gas diffusion to the grain boundaries. This requires the solution of a diffusion equation for the intragranular gas, which can be formulated as follows, for example [89]:

$$\frac{\partial C}{\partial t} = D\nabla^2 C + \beta, \tag{3.9}$$

where C is the concentration of gas atoms, D the diffusion coefficient of gas atoms and β the gas atom production rate.

Forsberg and Massih [89] derived an approximate integral solution to this differential equation. This has become known as the Forsberg-Massih model of fission gas release, and it has been implemented in many fuel performance codes such as FRAPCON [67] and BISON [70]. Later, Hermansson and Massih [83] updated this approximate solution with an additional term, and this is solution used in FINIX for the intragranular diffusion. In the diffusion equation, a term describing redissolution from grain boundaries appears which would require the intra- and intergranular models to be solved simultaneously. In order to simplify the solution, this redissolution term is neglected. However, redissolution along with trapping is taken into account in the effective diffusion coefficient of the model, calculated from the gas atom diffusion coefficient in trap-free media and

Table 3.1. Typical processes considered in a fission gas release model according to Blair [81] and whether these processes are considered in the fission gas release model implemented in FINIX in Publication V.

Process	In FINIX	
Gas production	Yes	Linear relationship with power density [82]
Recoil and knockout	No	
Intragranular diffusion	Yes	Approximate solution by Hermansson and Massih [83] using the three-term Turnbull diffusion coefficient [84, 85]
Intragranular bubble formation and behavior	Yes	Bubble number density and radius from White and Tucker [86], bubble diffusion coefficient of van Uffelen et al. [87] is used and trapping included in effective diffusion coefficient
Intergranular bubble formation and behavior	Yes	Model by Pastore et al. [76]
Irradiation-induced redissolution	Partially	Redissolution from grain boundaries not implemented in order to solve the intra- and intergranular behavior separately [88, 5], intragranular bubble redissolution from Massih and Forsberg [82]

the bubble diffusion coefficient as

$$D_{\text{eff}} = \frac{b}{b+g} D_{\text{atom}} + \frac{g}{b+g} D_{\text{bubble}}, \tag{3.10}$$

where b is the rate of irradiation-induced redissolution of gas atoms, g the trapping rate of gas atoms into intragranular bubbles, D_{atom} is the gas atom diffusion coefficient and D_{bubble} is the bubble diffusion coefficient. D_{atom} is dependent on temperature through an Arrhenius-type relationship, but also on fission rate [86]. The relationship with fission rate is caused by the effect fission fragment damage has on gas atom diffusion [86].

The intragranular model is used to provide the grain boundary fission gas inventory as a boundary condition for the intergranular model. The intergranular model follows closely the model developed by Pastore et al. [76]. The model describes the evolution of grain boundary vacancy and gas atom concentrations as well as the amount and size of grain boundary bubbles. The release criterion is based on fractional coverage, F_c, of the grain faces, defined as

$$F_c = N_{gb} A_{gb}, \tag{3.11}$$

where N_{gb} is the number density of grain boundary bubbles and A_{gb} the average area of a grain boundary bubble.

Irradiation-induced redissolution[2] from grain boundaries is not implemented in FINIX in order to solve the intra- and intergranular behavior separately [88, 5]. However, irradiation-induced redissolution of intragranular bubbles is taken into account, as described with the effective fission gas diffusion coefficient.

3.3.5 Cladding plasticity

In the following discussion, the permanent deformation of the cladding is divided into two parts: the time-independent, instantanous plasticity, and creep, which is time-dependent.

At low temperatures, zirconium appears in the α-phase, which has a hexagonal close packed (hcp) crystal structure, and the unit cell is a hexagonal prism. In the hcp phase, the texture, the orientation of the grains, of zirconium affects the macroscopic behavior of the material [90]. At higher temperatures, zirconium appears in the β-phase, which has a body centered cubic structure. The β-phase has important implications in accident conditions, which are not covered in this work.

The material property correlations implemented in FINIX regarding cladding plasticity in Publication V are empirical models and based on macroscopic observations of material behavior. In these models, the macroscopic behavior is not related to microscopic processes, but has a mathematical form that best reproduces the macroscopic behavior. In any case, also the microscopic behavior of zirconium is different in instantaneous and time-dependent plasticity or creep. The major microscopic process behind (time-independent) plastic deformation in α-zirconium is thought to be dislocation slip, although twinning may also play a significant role [90]. Creep, on the other hand, is thought to occur due to other processes such as dislocation climb and glide, with additional processes in irradiation creep [91].

Time-independent, instantaneous plastic deformation is thought to occur when a selected measure of stress exceeds the yield strength of the material. When stress occurs only in one direction, this stress can be used directly, however, when the stress is multiaxial the definition of a representative stress value is more complicated. The most commonly used measure is the von Mises effective stress, which in the absence of shear stresses is defined as follows, with i being an index over the dimensions:

$$\sigma_e = \sqrt{\frac{3}{2}\sum_i s_i s_i}, \tag{3.12}$$

where s_i is the deviatoric stress, defined as

$$s_i = \sigma_i - \frac{\sum_i \sigma_i}{3} = \sigma_i - p_{hs}. \tag{3.13}$$

[2]In fission gas release literature, the terms resolution or re-solution are used. In this context, *to resolute* means *to dissolve again*, for which the correct noun is redissolution.

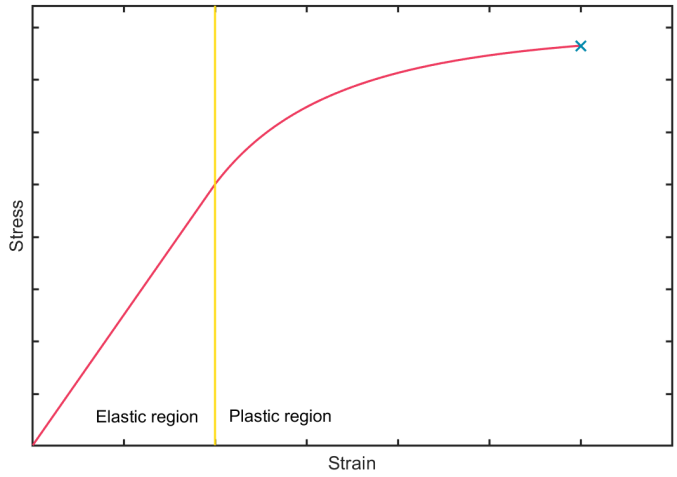

Figure 3.4. A typical stress-strain curve. Deformation in the elastic region is linearly dependent on stress and reversible, and in the plastic region the deformation is irreversible. The material shown is hardening, with a nonlinear stress-strain relationship above the elastic region. The cross marks the point in stress-strain space where the material fails.

where the second term, defined as p_{hs}, is the hydrostatic stress. Yielding based on effective stress assumes that yielding occurs as a critical elastic shear energy is achieved [92]. The difference between the stress measure and the yield strength is called the yield function, and using the von Mises effective stress we get the von Mises yield function:

$$f(\sigma_e, \epsilon_e) = \sigma_e - \sigma_Y(\epsilon_e), \tag{3.14}$$

where σ_Y is the yield strength, ϵ_e is the effective strain and σ_e is the von Mises effective stress.

In FINIX, the yield strength is calculated for Zircaloy from a correlation fitted to experimental data [93, 94]. When the yield strength is exceeded, the resulting effective strain is calculated by the radial return algorithm, which is described in Publication V. The radial return algorithm is an implicit integration algorithm of the plasticity equations [92], and as such is widely used. Several typical approximations are made in order to solve the equations effectively, such as imcompressibility and isotropicity of the cladding and the applicability of the Prandtl-Reuss flow rule[3]. Although the real behavior of materials deviates

[3]The Prandtl-Reuss flow rule relates the effective plastic strain to the individual plastic strain components using deviatoric stress, and for a strain increment $d\epsilon_i$ it is defined as:

$$\mathrm{d}\epsilon_i = \frac{3}{2}\frac{s_i}{\sigma_e}\mathrm{d}\epsilon_e.$$

slightly from that predicted by the Prandtl-Reuss equations behind the flow rule, its accuracy is sufficient for engineering applications [95].

In contrast to time-independent plastic deformation, cladding creep is permanent deformation under stress which is lower than the yield stress of the material. There are several models in the literature describing this process, one of the most well-known being the Limbäck-Andersson creep model [96].

Creep can typically be divided into three phases: primary creep, where the strain rate is decreasing, secondary creep, where the strain rate is constant, and tertiary creep, where the strain rate is increasing and leads to failure of the material. In fuel performance codes, tertiary creep is typically neglected, and creep strain is thought to consist of the sum of primary and secondary creep strains:

$$\epsilon_c = \epsilon_{c1} + \epsilon_{c2}. \tag{3.15}$$

The primary creep rate is often thought to be dependent on the secondary creep rate, and the secondary creep rate is divided into thermal and irradiation creep. In FINIX, two models, the original Limbäck-Andersson model and a modification to it by Geelhood [97] are implemented. In both models, the primary creep strain is modeled with a function

$$\epsilon_{c1} = \epsilon_{c1}^{\text{sat}}(1 - \exp(f(\dot{\epsilon}_{c2})t)), \tag{3.16}$$

where $\epsilon_{c1}^{\text{sat}}$ is the saturated primary creep strain and t the time. With this function, the primary creep strain increment during a time step can be calculated by

$$\Delta\epsilon_{c1} = a\,(\epsilon_{c1}(t_1) - \epsilon_{c1}(t_0)), \tag{3.17}$$

where a is the direction of creep. The secondary creep strain increment, in turn, is calculated more simply using the the sum of the thermal and irradiation creep rates:

$$\Delta\epsilon_{c2} = b\left(\dot{\epsilon}_{c2,th} + \dot{\epsilon}_{c2,irr}\right)\mathrm{d}t, \tag{3.18}$$

The creep rates, both primary and secondary, are functions of a stress measure, fast neutron flux and fast neutron fluence. The models differ in how the directions of creep, a and b, are defined, as well as the used stress measure.

The original Limbäck-Andersson model uses the hoop stress as the stress measure, and the directions of both primary and secondary creep are the direction of hoop stress, i.e.

$$a = b = \frac{|\sigma_\theta|}{\sigma_\theta}. \tag{3.19}$$

The Geelhood modification to the model was made in order to better predict creep behavior in transient conditions [97]. Basically, the most important modifications included the use of effective stress change[4] as the stress measure for the calculation of primary creep, whereas the calculation of secondary creep is as in the original model. In addition, the directions of the creep are defined based on

[4]Small changes in effective stress are ignored as only changes larger than 5 MPa are taken into account.

these stress measures so that the sign of the effective stress change determines the direction of primary creep, and hoop stress the direction of secondary creep, i.e.

$$a = \frac{|\Delta\sigma_{\mathrm{e}|}}{\Delta\sigma_{\mathrm{e}}}, \text{ and} \tag{3.20}$$

$$b = \frac{|\sigma_\theta|}{\sigma_\theta}, \tag{3.21}$$

Two Halden creep tests were used in the validation of the implementation of these models. In IFA-585 [98], a Zircaloy-2 cladding tube was held at several stress levels under irradiation, and in IFA-699 [99] a similar treatment with a simpler stress history was done for a Zircaloy-4 rod. In figure 3.5 the results from this validation are shown. Even though the agreement with experimental results is not perfect, this is typical of these common models, as can be seen from [100], for example.

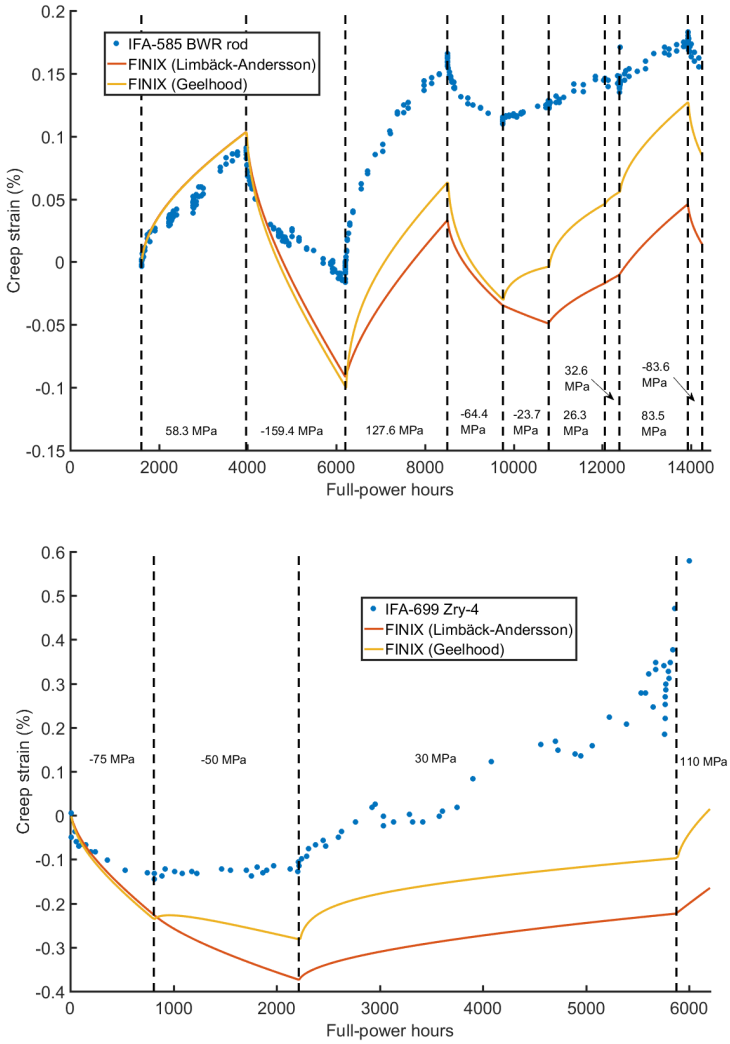

Figure 3.5. FINIX creep model predictions compared to Halden creep experiment results. Upper figure shows results from the simulation of the IFA-585 test, and lower figure from the IFA-699 test. Figures reproduced from Publication V.

3.4 Integral validation

Several Halden experiments have been used in the integral validation of fuel temperatures. In the Halden tests, an instrumented fuel assembly has been irradiated for a period of time equipped with thermocouples or an expansion thermometer. The results from these measurements can then be compared with FINIX predictions. In the first FINIX validation in Publication IV, data from OECD/NEA International Fuel Performance Experiments database [101] is used, specifically the Halden tests IFA-429 and IFA-432. In later validations, the data is directly obtained from Halden and condensed with the FuelRod Analysis Toolbox [102]. Data condensation is necessary, as Halden reports measurements typically at 15-minute intervals, and such an interval yields a very large dataset over an irradiation lasting multiple years. Data condensation aims to reduce the number of data points while preserving the initial data, practically by fitting a piecewise linear approximation to the initial data.

In addition to data treatment, the number of validation cases was increased. In the validation in Publication V, data from newer Halden tests IFA-515, IFA-677 and IFA-681 is also included. All in all ten rods were included in the validation, and the details of these rods are shown in table 3.2. The validation results show that the scatter in experimental versus predicted temperatures was greater in the older Halden tests, whereas it was not so in the newer Halden tests. The data from older and newer tests are shown separately in figure 3.6 regarding fuel centerline temperature.

The fission gas release model predictions of FINIX have been validated with data from Halden experiments (IFA-429, IFA-677.1 and IFA-681), data from the OECD/NEA IFPE database (ANO-2 and BR-3 rods) [101] and publicly available data (DR-3 [103] and Oconee [104]). Comparison to experimental data of fission gas release is shown in table 3.3. Even though small predicted fission gas releases are quite close to experimental values, high fission gas releases are underestimated. Inclusion of new models such as pellet micro-cracking is thought to increase fission gas release in these cases.

Table 3.2. The rods irradiated in Halden experiments included in the FINIX temperature validation. Burnup refers to rod-average end-of-life burnup.

Rod	Clad type	Burnup ($MWd \cdot kg_U^{-1}$)	Ref.
IFA-429 rod BC	Zry-4	60.2	[101]
IFA-432 rod 1	Zry-2	30.6	[105, 106, 101]
IFA-432 rod 2	Zry-2	44.2	[105, 106, 101]
IFA-432 rod 3	Zry-2	44.2	[106, 101]
IFA-432 rod 5	Zry-2	46.5	[106, 101]
IFA-515.10 rod A1	Zry-2	86.4	[107]
IFA-515.10 rod B1	Zry-2	95.4	[107]
IFA-677.1 rod 2	Zry-4	29.7	[108]
IFA-681 rod 1	Zry-4	41.1	[109, 110]
IFA-681 rod 5	Zry-4	40.5	[109, 110]

Table 3.3. Fission gas release validation results comparing the predicted values by FINIX to the experimental data.

Rod	FGR (%)		Ref.
	Pred.	Exp.	
ANO-2 TSQ002	2.51	1.00	[101]
DR-3 pa29-4	30.6	48.1	[103]
DR-3 m2-2c	25.7	35.6	[103]
BR-3 30i8	10.9	34.5	[101]
BR-3 36i8	14.7	33.8	[101]
BR-3 111i5	4.04	14.4	[101]
BR-3 24i6	10.7	21.8	[101]
BR-3 28i6	5.85	13.2	[101]
IFA-429 rod DH	31.6	57.4	[105]
IFA-681 rod 1	4.20	2.09	[109, 110]
IFA-677.1 rod 2	9.84	19.7	[108]
Oconee 15309	2.05	0.80	[104]

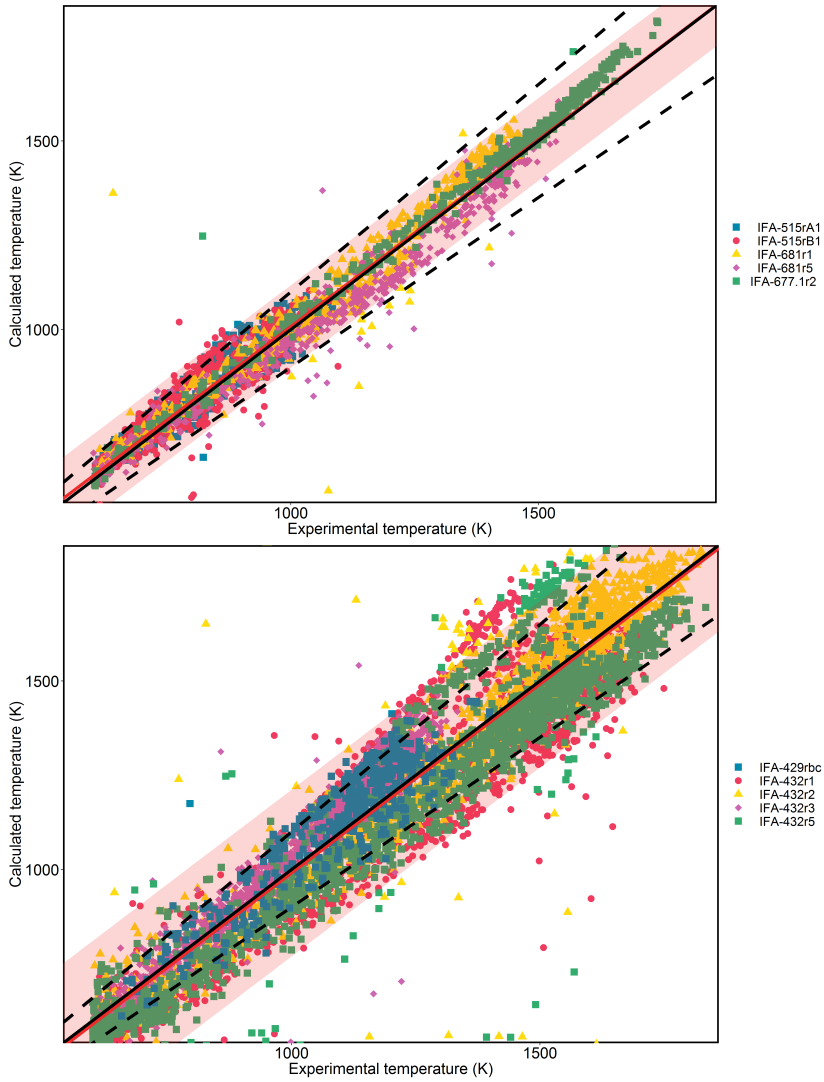

Figure 3.6. FINIX temperature predictions compared to experimental measurements. Upper figure contains data from newer Halden tests IFA-515, IFA-677 and IFA-681. Lower figure contains data from older Halden tests IFA-429 and IFA-432. Figures reproduced from Publication V. Dashed lines show ±10% deviation from perfect agreement, and the red line is a regression line fitted to the data. The red shaded area shows the prediction interval.

4. Uncertainty analysis of nuclear fuel behavior

4.1 Background

The predictions of a fuel performance code – as applies to the result from any computational model – contain uncertainties that can be traced back to various sources. For example, the manufacturing parameters such as dimensions and densities are not exactly the same from rod to rod, but vary according to a distribution. In fuel behavior analysis, the exact value of a manufacturing parameter for a certain rod is often not known, but these distributions over a set of rods are. In addition, the models within a fuel performance code contain parameters that are fitted to some experimental data, such as material properties of the pellet and the cladding. From the experimental data they are based on and the scatter in experimental data used in deriving these correlations, these parameters are also uncertain to some degree.

There are many ways to classify the uncertainty in modeling. One such division, as mentioned by Oberkampf [111], is the division into aleatory and epistemic uncertainty, where the former refers to the inherent variability in the input values and mathematical representation, and the latter to uncertainty from lack of knowledge of the physical system. In another classification by Kennedy and O'Hagan [112] variation in the model inputs such as manufacturing parameters is referred to as parametric variability of the model, whereas the uncertainty of model parameters is referred to as the parametric uncertainty.

Additionally, the results calculated by a model can be biased. The amount of bias should be determined from model validation, for example, by calculating the prediction error against the validation dataset. The bias contains also a degree of uncertainty, as from validation case to validation case the prediction error is different, and the experimental data the prediction error is based on contains its own uncertainties.

In practice, a Monte Carlo approach is typically suitable for nuclear fuel uncertainty analysis. Such analysis is performed by successive simulation runs where the input parameters, be they fuel manufacturing parameters or fuel perfor-

mance code model parameters, are sampled from their respective distributions by simple random sampling. As a result, distribution of output parameters are obtained based on the distributions of the selected input parameters.

4.2 Interval estimation

The Nuclear Safety Guides (YVL) applied by the Finnish Nuclear and Radiation Safety Authority (STUK) allow the use of statistical methods to show that there is a 95 % probability that an examined parameter does not exceed the specified acceptance limit with 95 % confidence [113].

The requirement of the regulatory guide YVL B.3 can be satisfied by showing that the upper tolerance interval is below the specified acceptance limit. The upper tolerance interval, U, with parameters γ and β can be formulated mathematically as follows:

$$P\left(\int_{-\infty}^{\mathrm{U}} f(x)dx \geq \gamma\right) \geq \beta, \tag{4.1}$$

where $f(x)$ is the probability density function of a random variable x. With the notation above, the tolerance interval U is called the γ-content upper tolerance interval with a confidence level of β [114]. To be consistent with the regulatory requirement in YVL B.3, we must select $\gamma = \beta = 0.95$.

A method used widely in the nuclear industry in the determination of tolerance intervals is based on order statistics, a term coined by Wilks [115, 116]. Wilks showed that the distribution of the proportion of the population between two order statistics is independent of the sampled population [114]. The nonparametric nature of Wilks' proof makes the method applicable to any population, as one does not have to know the population parameters in order to apply the method. The order statistics of a sample are formulated simply by taking a sample X with N observations from a population,

$$X = (x_1, x_2, ..., x_N), \tag{4.2}$$

and arranging the observations in ascending order as follows:

$$Y = \left(y_1 = x_i, y_2 = x_j, ..., y_N = x_k\right) \tag{4.3}$$

where y_i are the order statistics of the sample and

$$x_i < x_j < ... < x_k. \tag{4.4}$$

4.3 Minimum sample size

When simulating a large number of rods, it is convenient to perform only the minimum number of replicate simulation runs with sampled input parameters

to determine the output parameter distribution. This is practically illustrated by the following calculation: The number of rods in a typical nuclear reactor core is in the order of 50 000 rods. Simulating one rod with a standalone fuel performance code may take from 5 seconds to minutes, depending on the type of simulation being done. With a simulation time of 15 seconds, one run across a single core requires over 200 CPU-hours. Therefore, for practical reasons, the possible number of simulation runs is limited.

Wilks used an equation similar to Eq. (4.1) to derive the minimum sample size required that the order statistic y_N is the upper tolerance limit with certain parameters γ and β. Eq. (4.1) can be written as

$$\beta = 1 - \sum_{j=s-r}^{N} \binom{N}{j} \gamma^j \left(1-\gamma\right)^{N-j} = 1 - I\left(\gamma; s, N-s+1\right), \tag{4.5}$$

where $I(x;a,b)$ is the regularized incomplete beta function [1] [117]. In the case of the upper tolerance interval, if we set $r = 0$ and $s = N$, we obtain the so-called (first-order) Wilks' formula:

$$\beta = 1 - \gamma^N, \tag{4.6}$$

from which the required sample size can be solved. For $\gamma = \beta = 0.95$, the required number of samples N is 59. The specifier first-order for the Wilks' formula results from setting $s = N$. Setting $s = N - 1$ results in the second-order formula and so on.

4.4 Missing data in order statistics methods

In any computational model, it is probable that given a number of initial conditions the model does not converge to a solution for some of the initial conditions. This is also true with fuel performance codes, but it brings about a problem when using order statistics methods. With a failed simulation, we do not know which order statistic the failed simulation would have been had it succeeded. Especially in the case of tolerance limits, the failed simulation could very well be the highest order statistic. This problem is well-known in statistics as missing data [118]. Missing data is typically categorized by the reason the data is missing: it may be missing completely at random, missing at random or not missing at random [119, 118]. The last is most difficult, as the missing data may be similar and their exclusion from the dataset would lead to bias in the results.

For a conservative approach, we should assume that failed fuel performance simulations do not appear at random, and so the unobtained results from these simulations could be extreme values. Since in our case we wish to know a

[1] The regularized incomplete beta function is defined as the ratio of the incomplete beta function, $B(x;a,b)$ to the complete beta function $B(a,b)$ so that $I(x;a,b) = \frac{B(x;a,b)}{B(a,b)}$. The incomplete beta function is defined as $B(x;a,b) = \int_0^x t^{a-1}(1-t)^{b-1}\,dt$, which yields the complete beta function with the parameter $x = 1$.

limiting value, the tolerance interval, we may bias our dataset so that the calculated tolerance interval is higher than the real tolerance interval without any missing data. Imputation methods for missing data treatment are based on replacing the missing data with another, suitable data point [118]. In our case, worst-case imputation will preserve the nature of the tolerance interval. When calculating only summary statistics, numerical values can also be imputed. However, this is only possible with certain parameters, such as fission gas release, which as a relative quantity has an upper limit of 100 %, or cladding failure, which as a categorical quantity has a worst-case value of "failed". For a mean fission gas release in an assembly, one imputed worst-case fission gas release only has a small effect. For continuous quantities such as pressure or temperature, worst-case imputation is not possible.

However, we can also avoid this problem completely by using a higher-order Wilks' formula. Assuming that the failed simulations are the highest order statistics, we may exclude them and the tolerance interval is obtained from the highest actually calculated data point.

There is an upper limit for the number of failures that can be accounted for with this kind of method. As a larger number of samples must be obtained for one additional sample to be excluded, the increase in number of samples is a limiting factor. However, the number of additional samples required decreases with the number of samples taken, so the allowed failure rate increases. This is illustrated by figure 4.1. The allowed failure rate is defined by

$$r_{\text{fail}} = \frac{k}{N}, \tag{4.7}$$

where k is the order of the formula minus one.

The failure rate is a useful tool to estimate from an initial calculation run whether the use of the method is possible by calculating the ratio of the number of failed simulations to total number of simulations. If this ratio is higher than r_{fail} for any reasonable N, the method cannot be used.

4.5 Application to spent fuel disposal

The source term of radionuclides in spent fuel is important for the safety analyses of geological disposal of spent nuclear fuel. Roughly speaking, two processes determine the release of radioactivity: the dissolution of the uranium oxide matrix and the dissolution of the grain boundary and gas gap fission product inventory [120]. The latter is called the instant release fraction (IRF), defined as such because the gap inventory is readily available to the leaching water and the grain boundaries are thought to be leached before the dissolution of the fuel matrix [120]. The IRF contains radionuclides that are both long-lived and geochemically mobile, such as ^{129}I, ^{137}Cs, ^{35}Cl and ^{14}C, so it is important in determining the radiation dose caused by the final repository [120].

To some extent, the IRF of some nuclides, such as iodine and cesium isotopes,

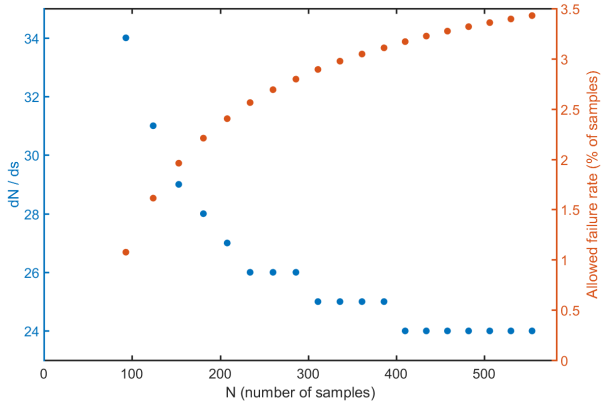

Figure 4.1. The number of allowed failed simulations as a function of the number of samples (red). With the first-order Wilks' formula (N = 59), no failed simulations are allowed. The number of additional samples required by the next-order formula are also shown (blue).

can be correlated with fission gas release after the irradiation of the fuel. Johnson et al. [120] suggest full-core fission gas release calculations to estimate the IRF, and such calculations have been performed for SKB, for example, by Oldberg [121] regarding the Oskarshamn NPP and by Nordström [122] regarding the Ringhals NPP. Such calculations yield fission gas release results which may or may not be conservative. In full-core fission gas release calculations, some rods are bound to have high fission gas releases, whereas the bulk of the rods may have quite low fission gas release values. In other words, the distribution of fission gas release as calculated by fuel performance codes has a long tail, as depicted in figure 4.2.

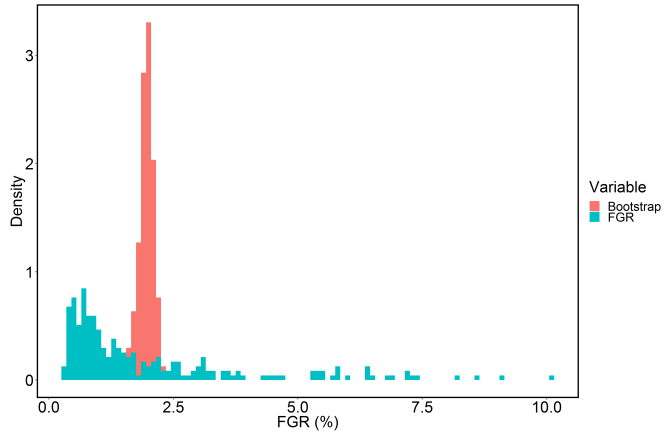

Figure 4.2. The distribution of fission gas release across rods in a hypothetical assembly compared to the bootstrapped mean values, depicting the variation of assembly mean fission gas releases in similar assemblies.

In final disposal, the individual rod fission gas releases are not important; the assembly fission gas release or even the final disposal capsule – which contains several assemblies – fission gas release are. A suitable summary statistic must then be selected from this data to depict the fission gas release across a hundred or more fuel rods. Maximum fission gas release in an assembly would be very conservative, as such values occur only in a few rods. Due to the threshold nature of fission gas release [123], if the fuel rods are operated near a threshold temperature, the fission gas release values may have a large scatter among the rods. The mean fission gas release is a much better statistic, and it is also substantially smaller than the maximum value, as shown in figure 4.2. The conservativeness of such a statistic can be analyzed through statistical simulations and the determination of a tolerance limit of the mean values.

One must also take into account all the relevant sources of uncertainty in such calculations. In figure 4.3, a comparison of output distributions obtained by varying different types of parameters are shown. The model parameter variation, in this case the ENIGMA fission gas effective diffusion coefficient, causes larger scatter than the variation in the fuel manufacturing parameters such as dimensions and pellet grain size. Also, the mean values obtained from each distribution are different. However, due to the non-additive nature of fuel performance code models [124], varying both models at the same time cause also the mean of the distribution, where all parameters are varied, to shift.

In Publication VI, an example case with idealized data based on the US PWR 16×16 case from the OECD/NEA IFPE database [101] is calculated. Power histories for a hypothetical assembly with 236 rods were generated from the available data for 9 rods in the database, and the fission gas releases calculated for each rod in the assembly. Each rod was calculated 59 times as specified by Eq. (4.6) and associated with an assembly-level sample. From these individual rod fission gas release values, 59 assembly means were obtained, and due to Eq. (4.6) the highest of these means was the upper tolerance interval of the mean fission gas release. In practice, a similar procedure can be done for complete reactor cores containing hundreds of assemblies.

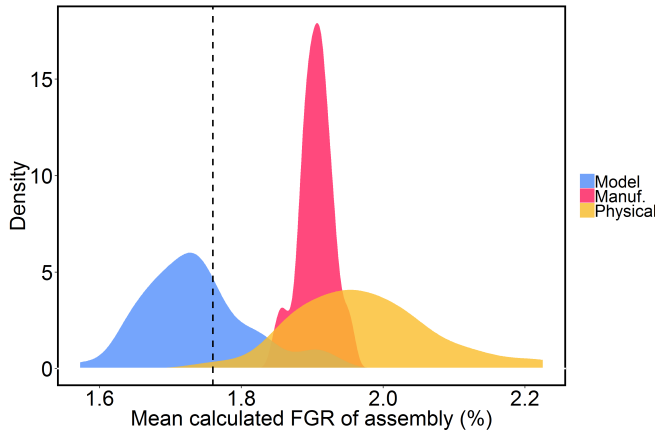

Figure 4.3. Comparison of the distributions, as kernel density estimates, of assembly mean fission gas releases when different parameter combinations are varied in the statistical simulations. Model refers to ENIGMA model parameters, Manuf. to fuel manufacturing parameters such as dimensions and Physical to the combination of Model and Manuf. Figure from Publication VI.

5. Conclusions

5.1 Nuclear fuel thermochemistry

Thermochemical modelling tools for nuclear fuel are developed in the first part of this thesis. An equilibrium solver developed by the author is applied into modelling oxygen potential of irradiated fuel as well as release of corrosive chemical species from the fuel. The modeling of these microscale phenomena could be used to inform modeling at the engineering level, improving existing models and yielding new insights.

In Publications I and II, the validation and verification of the thermochemical calculations on nuclear fuel are mainly dealt with, with a special emphasis on the prediction of the oxygen potential of the fuel. Publication I presents calculated results on uranium oxide and these are shown to agree with experimental results from the literature such as the phase boundary of the nonstoichiometric uranium dioxide and U_4O_9 and the oxygen potential of nonstoichiometric uranium dioxide. In Publication II, the predictions of the calculations on irradiated fuel are also shown to agree with experimental results from the literature.

However, varying the initial composition of the fuel showed interesting behavior of the oxygen potential. Typically, the oxygen potential of nuclear fuel is thought to only rise with burnup. Often, the initial oxygen-to-metal ratio of fuel is assumed to be stoichiometric, exactly 2, whereas realistically it is typically hyperstoichiometric, slightly above 2, in typical LWR fuel. For this slightly hyperstoichiometric fuel, the thermochemical calculations in Publications I and II show that initially the oxygen potential of fuel would fall, and only then begin to rise. For a realistic description of the chemical behaviour of nuclear fuel, such behaviour should be verified from experiments. In the literature, data are comparatively scarce, and the available data points cannot be used for such a comparison as the local elemental composition is often unknown. In addition, the calculations performed here assume a local thermochemical equilibrium, which is typically not a very good approximation in solid materials. The validity of this approximation in different conditions requires also experimental verification.

The agreement between the calculated results and experimentally determined oxygen potentials from a single fuel sample in Publication II are promising in this respect.

The kinetically constrained thermochemical calculations in Publication III aim to investigate the release of corrosive species from fuel under irradiation. These studies found that apart from unreactive cesium iodide, hydrogen iodide may also form in the pellet-cladding gap of nuclear fuel. Hydrogen iodide is reactive towards zirconium and might also contribute to stress-corrosion cracking of the cladding. In Publication III only hydrogen produced during irradiation is considered, but hydrogen as an impurity is probably also present in much larger amounts in fuel pellets. The impurity hydrogen would result in more hydrogen iodide being possibly formed, and more reactive iodine being released.

5.2 Nuclear fuel thermomechanics

The second part of the thesis focuses on the development of the fuel behaviour module FINIX, which can be applied at the engineering level for fuel performance analysis especially in simulations coupled to other reactor core physics solvers. At the outset, the predictions of FINIX regarding fuel temperatures during long irradiation periods were somewhat inaccurate at higher burnups. At higher burnups, various phenomena such as fuel swelling and densification, cladding creepdown and fission gas release affect the thermal behavior of the rod, and these models were not present in FINIX. Most such models required for better thermal predictions are implemented in FINIX as part of this thesis. The models selected for implementation were selected based on the models either being industry standards or state-of-the-art, but also based on the simplicity of the models. As FINIX is designed for coupled applications, the selected models must be computationally simple so that running time of the code can be optimized in coupled calculations.

The models implemented by the author in FINIX include six models describing the behavior of the fuel pellet and cladding. For the part of fuel pellet, fuel pellet swelling and densification models are implemented, the former generally decreasing fuel temperatures and the latter increasing them. A model for fission gas release from the pellet is implemented, which has effects on both the mechanical and thermal predictions, as fission gas release increases the internal pressure of the rod and decreases the thermal conductivity of the fill gas. The radial power distribution model decreases the temperature calculated for the centerline of the fuel pellet, where temperature is typically measured in an instrumented rod. This occurs due to the fact that the radial power distribution is peaked at the fuel pellet surface and slightly depressed at the centerline. For the part of the cladding, plasticity and creep models are implemented to calculate permanent deformation of the cladding under varying conditions. Especially the creep model influences the thermal predictions, as the pressure differential

across the cladding causes the cladding to creep down and decrease the pellet-cladding gap in long irradiations, lowering the centerline temperatures predicted by the code.

As a result of the development in this part of the thesis, FINIX temperature predictions are improved to correspond with other, state-of-the-art codes developed elsewhere. The current version of FINIX can now reliably be used in modeling fuel temperature during long irradiation periods.

5.3 Uncertainty analysis of nuclear fuel behavior

The third part of the thesis focuses on uncertainty analysis of the predictions obtained from fuel performance codes, with the specific application of predicting the state of spent fuel destined for final disposal. The fission gas release is a quantity whose calculation is an important part of fuel performance analysis, and it can be correlated with the instant release fraction of some important radionuclides such as ^{129}I and ^{137}Cs. However, there are uncertainties in the fission gas release predictions of fuel performance codes associated with the uncertainties in the manufacturing parameters of the fuel rods as well as the models in fuel performance codes. Taking into account these uncertainties, limiting values for the fission gas release can be calculated.

In the application to final disposal of spent fuel, the fuel is treated as complete assemblies rather than individual fuel rods. A single fuel performance simulation, however, can only simulate a single fuel rod, so several fuel performance simulations have to be summarized in order to get an assembly-level statistic. The mean is selected as the suitable statistic for an assembly, and a limiting value for the mean is calculated. The uncertainty analysis methodology developed in this thesis is based on order statistics and as such can be used to determine an upper tolerance limit for fission gas release in complete assemblies. The methodology developed in this part of the thesis can now be used to obtain fission gas release predictions for full reactor cores and used in day-to-day engineering applications.

Appendices

A Validation of burnup calculations

In the following figures, the mole amounts of elements calculated for the rod investigated by Walker et al. [22] for the work in Publication II are compared to the experimental results. The results calculated by Serpent at a cooling time of 10 years are shown. In addition, results calculated by Piro et al. [33] with ORIGEN are shown for the local elemental compositions.

Walker et al. [22] measured both the average elemental composition of the fuel with ICP-MS and the local elemental concentrations along the pellet radius with EPMA (electron probe microanalysis) for the following elements: Nd, Cs, Pu, Kr and Xe. Local elemental concentrations for the remaining elements have also been estimated by assuming the concentration of Nd correlates with burnup.

Walker et al. [22] report that not all of the fuel sample was dissolved when preparing the ICP-MS sample, but a metallic residue was left. The metallic residue can plausibly be thought to contain the elements present in the noble metal particles: Mo, Tc, Ru, Rh and Pd. Some other transition metals, such as Ag, Cd, Sn and Sb have also been reported as having been dissolved in these metallic particles [13]. This may explain the higher calculated amount seen in the following figures for the elements Mo, Tc, Ru, Rh, Pd, Sn and Sb. In all of the following figures the measured amount of xenon is lower than what has been calculated by either code, which most probably results from bubbles cut in the sample preparation stage losing their contents.

In addition to the pellet average composition, several local compositions were measured by Walker et al. [22] with EPMA. The results reported by Piro et al. [33], calculated with ORIGEN, are also shown for radial locations of 0.5, 0.8 and 0.975. Difference between Serpent and ORIGEN at r = 0.5 and 0.8 is small, but at r = 0.975 there is a slightly larger difference. The amounts of fission products are calculated by ORIGEN to be higher and the amount of Pu slightly lower.

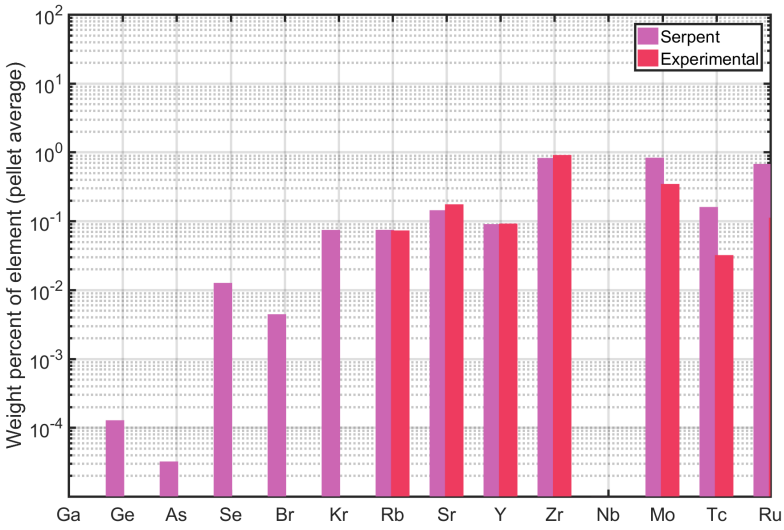

Figure A.1. Comparison with pellet average element composition from Walker et al. [22] for fission products from Ge to Tc.

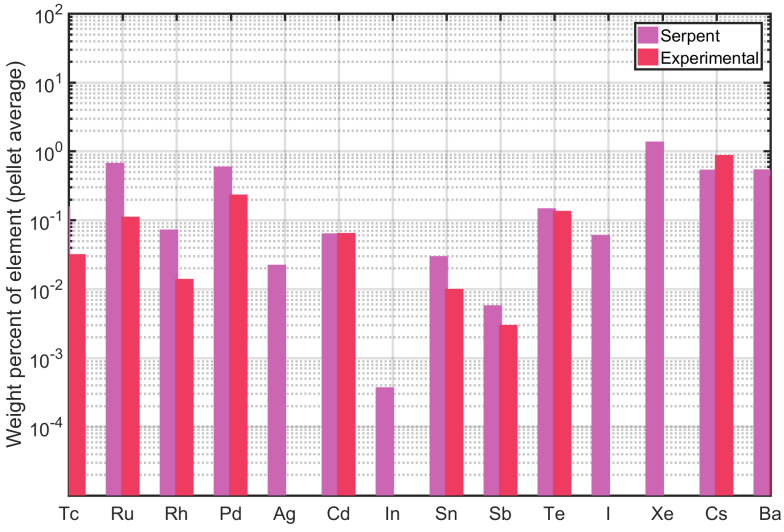

Figure A.2. Comparison with pellet average element composition from Walker et al. [22] for fission products from Ru to Cs.

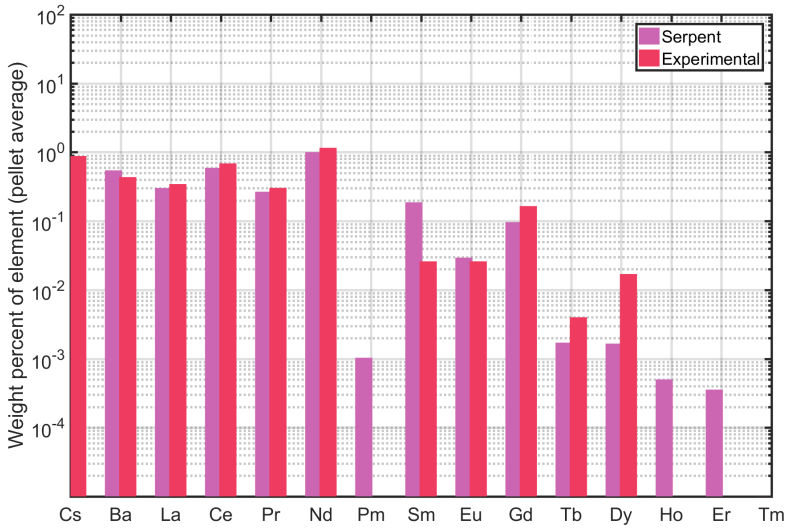

Figure A.3. Comparison with pellet average element composition from Walker et al. [22] for fission products from Ba to Er.

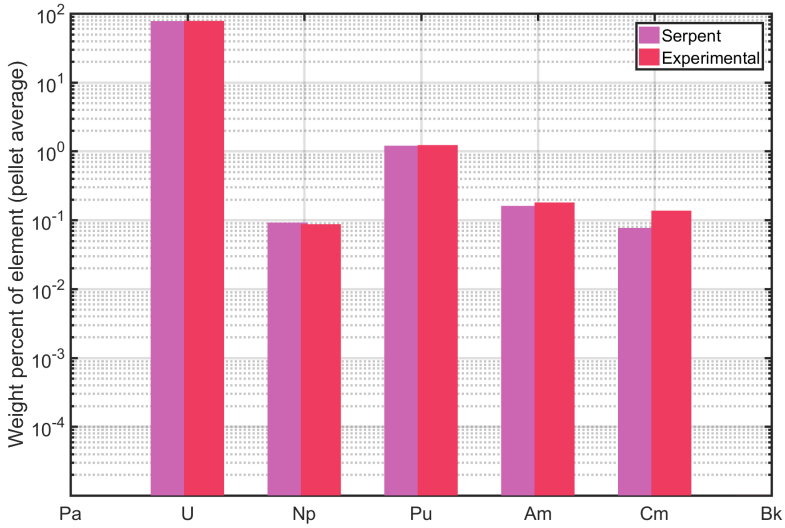

Figure A.4. Comparison with pellet average element composition from Walker et al. [22] for actinides.

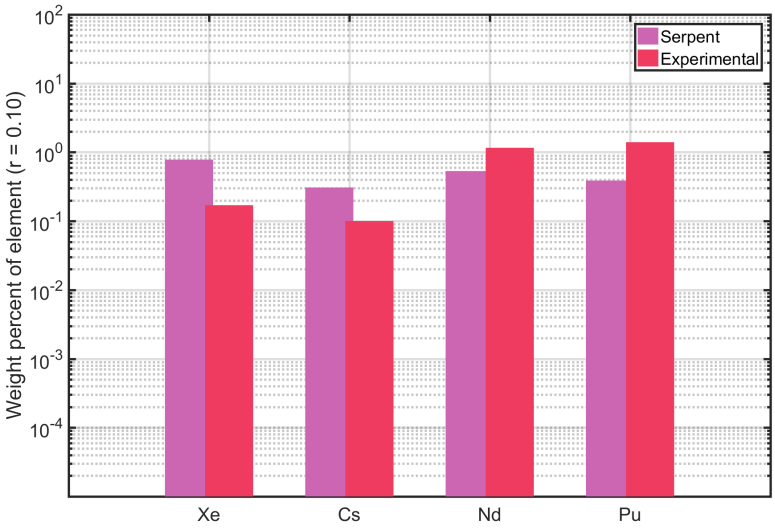

Figure A.5. Comparison with measured local element composition from Walker et al. [22] and calculated values from Piro et al. [33] at r = 0.1.

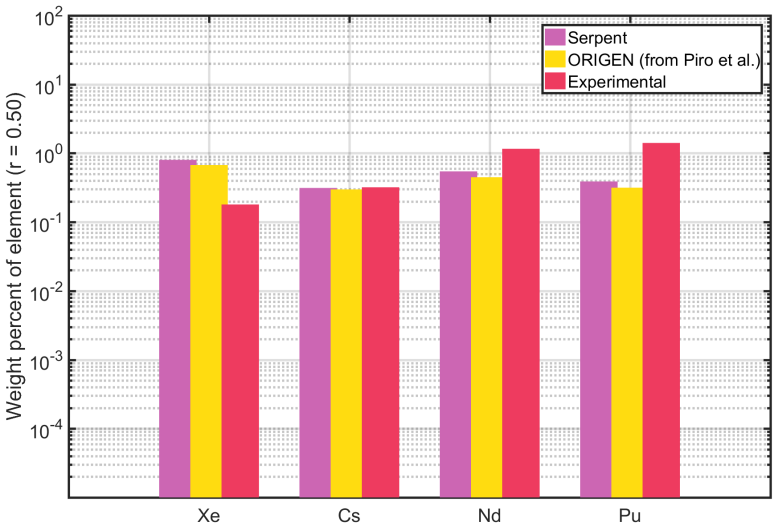

Figure A.6. Comparison with local element composition from Walker et al. [22] and calculated values from Piro et al. [33] at r = 0.5.

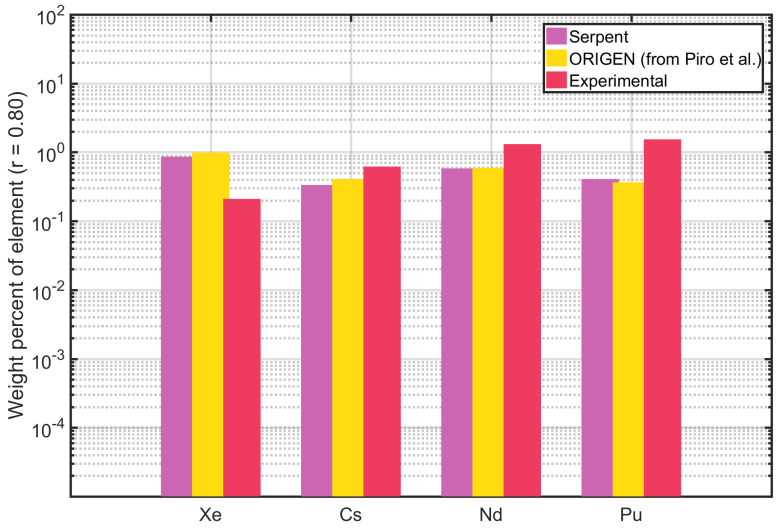

Figure A.7. Comparison with local element composition from Walker et al. [22] and calculated values from Piro et al. [33] at r = 0.8.

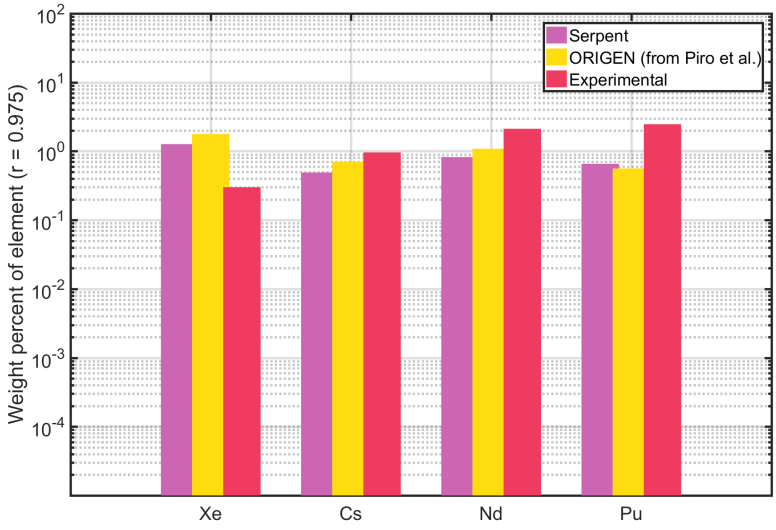

Figure A.8. Comparison with local element composition from Walker et al. [22] and calculated values from Piro et al. [33] at r = 0.975.

B Kinetic energy distribution of fission fragments on fuel surface

The following draws heavily from van Reenen and de Wet [62]. If a fission fragment is moving in the direction specified by $d\theta$ and $d\phi$ in spherical coordinates, the fraction of fission fragments generated at the center of the sphere moving in this direction is $\frac{1}{4\pi}\sin\theta d\theta d\phi$ if the fission fragments are generated isotropically. Additionally, the number of fission fragments generated in a layer with thickness dx is $2\dot{F}dx$. Here, $\dot{F}$ is the fission rate per unit volume and is taken as a constant.

These may be used to calculate the total flux of fission products escaping the surface, which is given by

$$\phi = \frac{\dot{F}}{2\pi}\int_{x=0}^{R}\int_{\theta=0}^{\cos^{-1}\left(\frac{x}{R}\right)}\int_{\phi=0}^{2\pi}\sin\theta dx d\theta d\phi = \dot{F}\int_{0}^{R}\left(1-\frac{x}{R}\right)dx = \frac{\dot{F}R}{2}. \quad \text{(B.1)}$$

The integration for ϕ is done over all angles, but for θ only from 0 the the angle with which the fission fragment with range R reaches the surface. The final form of this relation is also used by Konashi et al. [57].

The above equation does not give any consideration to the energies the fission products have on the fuel surface. One must therefore relate the integration limits in Eq. (B.1) to the energy. This may be done with a function defining the energy deposition of the fission fragment. For any ion, the following equation may be used:

$$E = E_0\left(1-\frac{z}{R}\right)^n, \quad \text{(B.2)}$$

where z is the path length of an ion traversing through the material and n an experimentally determined exponent, typically from 1 to 3. Several examples of the use of such equations are given by [125]. In the geometry discussed here, $z = \frac{x}{\cos\theta}$. Kahn, Harman and Forgue [126] have found that $n = 2$ fits experimental data for fission fragments best, so a relation

$$E = E_0\left(1-\frac{x}{R\cos\theta}\right)^2, \quad \text{(B.3)}$$

may be used. Eq. (B.3) is called the "square law" by Nguyen and Grossman [127].

The integration limits from Eq. (B.1) must be adjusted with the help of Eq. (B.3) to give the amount of fission fragments with energy between 0 and E. All angles in the plane of the surface may yield such fragments, so ϕ is integrated as in Eq. (B.1).

The integration limits for θ are the angle yielding fission fragments with $E_{\mathrm{ff}} = 0$ and angle yielding fission fragments with $E_{\mathrm{ff}} = E$. The upper limit is as in Eq. (B.1) and the latter is solved from Eq. (B.3) as

$$\theta_0 = \cos^{-1}\left(\frac{x}{R}\left(\frac{1}{1-\sqrt{\frac{E}{E_0}}}\right)\right). \quad \text{(B.4)}$$

With angles θ smaller than specified by Eq. (B.4), the fission fragments have energies greater than E and must not be counted. With these integration limits, the energy E appears as now a variable in the integral, as follows:

$$\phi = \frac{\dot{F}}{R}\left(\frac{\sqrt{\frac{E}{E_0}}}{1-\sqrt{\frac{E}{E_0}}}\right)\int x dx. \tag{B.5}$$

The integration with respect to x is conveniently done in two regions. Above a certain value of x, no angle θ yields energies greater than E at the surface. These fission fragments may be counted with Eq. (B.1). Below this limit, only the angles specified by the limits in Eqs. (B.1) and (B.4) yield fission fragments with energy equal or below E, and Eq. (B.5) must be used. This limiting value of x, x_{lim} may again be calculated from Eq. (B.3), setting $\theta = 0$ as fission fragments generated in the direction normal to the surface have the highest energy:

$$x_{\mathrm{lim}} = R\left(1-\sqrt{\frac{E}{E_0}}\right) \tag{B.6}$$

Now the integration over x may be performed from 0 to x_{lim} with Eq. (B.5) and from x_{lim} to R with Eq. (B.1), as follows:

$$\phi = \frac{\dot{F}}{R}\left(\frac{\sqrt{\frac{E}{E_0}}}{1-\sqrt{\frac{E}{E_0}}}\right)\int_0^{x_{\mathrm{lim}}} x dx + \dot{F}\int_{x_{\mathrm{lim}}}^{R}\left(1-\frac{x}{R}\right)dx$$

$$= \frac{\dot{F}R}{2}\sqrt{\frac{E}{E_0}}. \tag{B.7}$$

It is clear that the root in Eq. (B.7) results from the parameter fitted by Kahn et al. [126] in Eq. (B.3), but the result is very useful in its simplicity.

Dividing Eq. (B.7) by $2\dot{F}R$, we may obtain the cumulative distribution function of fission fragments. For calculation purposes we need the probability density function, for which we need to define the cumulative distribution function. It is obvious that half of all fission fragments have a direction away from the surface, and from Eq. (B.1) it results that half of the fission fragments directed towards the surface do not reach the surface. A partial probability distribution function can be obtained as

$$f_E = \frac{dF_E}{dE} = \frac{1}{8E_0}\left(\frac{E}{E_0}\right)^{-\frac{1}{2}}, \text{ when } 0 < E \le E_0. \tag{B.8}$$

If one wants to use the partial probability density function for calculations with only the fission fragments that reach the surface, it must first be normalized by multiplying with 4, neglecting the probability mass at $E = 0$.

Therefore, the pdf for the fission fragments that reach the surface is just

$$f_{E,\,\mathrm{surf}} = \frac{1}{2E_0}\left(\frac{E}{E_0}\right)^{-\frac{1}{2}}. \tag{B.9}$$

With this result, the average properties of the fission fragments can be obtained by integration, for example the energy at surface:

$$E_{\text{surf, ave}} = \int_0^{E_0} E f_{E,\,\text{surf}} dE = \frac{E_0}{3}. \tag{B.10}$$

References

[1] D Olander. *Fundamental Aspects of Nuclear Reactor Fuel Elements*. 1976.

[2] H Loukusa, T Ikonen, V Valtavirta, and V Tulkki. Thermochemical modeling of nuclear fuel and the effects of oxygen potential buffers. *Journal of Nuclear Materials*, 481:101–110, 2016.

[3] B Cox, B A Surette, and J C Wood. Stress corrosion cracking of Zircaloys in unirradiated and irradiated CsI. *Journal of Nuclear Materials*, 138:89–98, 1986.

[4] B Cox. Pellet-clad interaction (PCI) failures of zirconium alloy fuel cladding - A review. *Journal of Nuclear Materials*, 172(3):249–292, 1990.

[5] H Loukusa, J Peltonen, and V Valtavirta. FINIX – Fuel Behavior Model and Interface for Multiphysics Applications - Code Documentation for version 1.19.1. Technical Report VTT-R-00052-19, 2019.

[6] W T Thompson, B J Lewis, M H Piro, E C Corcoran, M H Kaye, J D Higgs, F Akbari, and D M Thompson. RMC Fuel Thermochemical Treatment, Appendix to: B J Lewis, W T Thompson, F C Iglesias, *Fission product chemistry in oxide fuels, chapter in:* Comprehensive Nuclear Materials, 1st edition, Ed: R J M Konings, 2012.

[7] T Ikonen. FINIX - Fuel behavior model and interface for multiphysics applications - Code documentation for version 0.13.9. Technical Report VTT-R-06563-13, VTT, Espoo, Finland, 2013.

[8] H Loukusa. Validation of the FINIX fuel behavior code version 0.13.9. Technical Report VTT-R-06565-13, VTT Technical Research Centre of Finland, Espoo, Finland, 2013.

[9] W J Kilgour, R J White, J H Shea, and J A Turnbull. The ENIGMA Fuel Performance Code Code Description Version 5.8d. Technical Report TD/NS/REP/0035, Nuclear Electric, 1992.

[10] V Tulkki. *Review of the Fuel Performance Code ENIGMA*. Lic.sc. (tech.) thesis, Aalto University School of Science, 2011.

[11] T Ikonen. Variance decomposition as a method of statistical uncertainty and sensitivity analysis of the fuel performance code FRAPCON-3.4. Technical Report VTT-R-07723-12, 2012.

[12] H Loukusa. *Computational module for the calculation of thermochemical equilibria in nuclear fuel*. M.sc. (tech.) thesis, Aalto University School of Chemical Technology, 2014.

[13] H Kleykamp. The chemical state of the fission products in oxide fuels. *J. Nucl. Mater.*, 131:221–246, 1985.

[14] L Johnson. A model for radionuclide release from spent UO_2 and MOX fuel. Technical Report NAB 13-37, NAGRA, Wettingen, Switzerland, 2014.

[15] J H Davies, E V Hoshi, and D L: Zimmerman. Ramp test behavior of high O/U fuel. *J. Nucl. Mater.*, 270:87–95, 1999.

[16] D Jädernäs, F Corleoni, A Puranen, P Tejland, and M Granfors. PCI mitigation using fuel additives. In *Proceedings of TopFuel*, pages 362–371, 2015.

[17] E H P Cordfunke and R J M Konings. *Thermochemical Data for Reactor Materials and Fission Products*. North-Holland, Amsterdam, Netherlands, 1990.

[18] E C Corcoran, M H Kaye, F Akbari, J D Higgs, B J Lewis, W T Thompson, R A Verrall, Z He, and J F Mouris. First principles CANDU fuel model and validation experimentation. In *Proceedings of the 2007 International LWR Fuel Performance Meeting*, pages 99–106, 2007.

[19] W T Thompson, B J Lewis, E C Corcoran, M H Kaye, S J White, F Akbari, Z He, R A Verrall, J D Higgs, D M Thompson, T M Besmann, and S C Vogel. Thermodynamic treatment of uranium oxide based nuclear fuel. *Int. J. Mat. Res.*, 98:1004–1011, 2007.

[20] E C Corcoran, M H Kaye, and M H A Piro. An overview of thermochemical modelling of CANDU fuel and applications to the nuclear industry. *Calphad: Computer Coupling of Phase Diagrams and Thermochemistry*, 55:52–62, 2016.

[21] Maria Pusa. *Numerical methods for nuclear fuel burnup calculations*. D.sc. thesis, Aalto University, 2013.

[22] C T Walker, V V Rondinella, D Papaioannou, S Van Winckel, W Goll, and R Manzel. On the oxidation state of UO_2 nuclear fuel at a burn-up of around 100 MWd/kgHM. *Journal of Nuclear Materials*, 345(2-3):192–205, 2005.

[23] J Leppänen, M Pusa, T Viitanen, V Valtavirta, and T Kaltiaisenaho. The Serpent Monte Carlo code: Status, development and applications in 2013. *Annals of Nuclear Energy*, 82:142–150, 2015.

[24] R Feynman. Illustrations of thermodynamics. In *The Feynman Lectures on Physics, Volume I*. California Institute of Technology, 2013.

[25] B Baurens, J Sercombe, C Riglet-Martial, L Desgranges, L Trotignon, and P Maugis. 3D thermo-chemical-mechanical simulation of power ramps with ALCYONE fuel code. *Journal of Nuclear Materials*, 452(1-3):578–594, 2014.

[26] B Baurens. *Couplages thermo-chimie-mecaniques dans l'UO_2 - Application a l'interaction pastille-gaine*. PhD thesis, Universite Aix-Marseille, 2014.

[27] P Konarski, J Sercombe, C Riglet-Martial, L Noirot, I Zacharie-Aubrun, K Hanifi, M Frégonèse, and P Chantrenne. 3D simulation of a power ramp including fuel thermochemistry and oxygen thermodiffusion. *Journal of Nuclear Materials*, 519:104–120, 2019.

[28] S Imoto. Chemical state of fission products in irradiated UO_2. *J. Nucl. Mater.*, 140:19–27, 1986.

[29] K Moriyama and H Furuya. Thermochemical Prediction of Chemical Form Distributions of Fission Products in LWR Oxide Fuels Irradiated to High Burnup. *Journal of Nuclear Science and Technology*, 34(9):900–908, 1997.

[30] M Mignanelli and R Thetford. Chemical modelling in TRAFIC. *Journal of Nuclear Materials*, 204:173–179, 1993.

[31] N E Bixler. VICTORIA 2.0: a mechanistic model for radionuclide behavior in a nuclear reactor coolant system under severe accident conditions. Technical Report NUREG/CR-6131, US NRC, 1998.

[32] M S Veshchunov, V D Ozrin, V E Shestak, V I Tarasov, R Dubourg, and G Nicaise. Development of the mechanistic code MFPR for modelling fission-product release from irradiated UO_2 fuel. *Nuclear Engineering and Design*, 236(2):179–200, 2006.

[33] M H A Piro, J Banfield, K T Clarno, S Simunovic, T M Besmann, B J Lewis, and W T Thompson. Coupled thermochemical, isotopic evolution and heat transfer simulations in highly irradiated UO_2 nuclear fuel. *Journal of Nuclear Materials*, 441(1-3):240–251, 2013.

[34] J W Gibbs. On the equilibrium of heterogeneous substances. *Trans. Conn. Acad. Arts Sci.*, 3:108–248,343–520, 1874.

[35] W R Smith and R W Missen. *Chemical Reaction Equilibrium Analysis: Theory and Algorithms*. Krieger Publishing Company, Malabar, FL, USA, 1991.

[36] W B White, S M Johnson, and G B Dantzig. Chemical Equilibrium in Complex Mixtures. *The Journal of Chemical Physics*, 28(5):751–755, 1958.

[37] Stuart R. Brinkley. Calculation of the Equilibrium Composition of Systems of Many Constituents. *The Journal of Chemical Physics*, 15(2):107, 1947.

[38] G Eriksson. Thermodynamic studies of high temperature equilibria. XII. SOLGASMIX, a computer program for calculation of equilibrium compositions in multiphase systems. *Chem. Scripta*, 8:100–103, 1975.

[39] G Eriksson. Thermodynamic studies of high temperature equilibria. III. SOLGAS, a computer program for calculating the composition and heat condition of an equilibrium mixture. *Acta Chem. Scand.*, 25:2651–2658, 1971.

[40] G Eriksson and E Rosén. Thermodynamic studies of high temperature equilibria. VIII. General equations for the calculation of equilibria in multiphase systems. *Chem. Scripta*, 4:193–194, 1973.

[41] W R Smith. Computational aspects of chemical equilibrium in complex systems. volume 5 of *Theoretical Chemistry: Advances and Perspectives*, pages 185–259. 1980.

[42] C F Weber. Convergence of the equilibrium code SOLGASMIX. *J. Comput. Phys.*, 145:655–670, 1998.

[43] P Koukkari. *Introduction to constrained Gibbs energy methods in process and materials*. VTT Technical Research Centre of Finland, Espoo, Finland, 2014.

[44] M H A Piro, T M Besmann, S Simunovic, B J Lewis, and W T Thompson. Numerical verification of equilibrium thermodynamic computations in nuclear fuel performance codes. *Journal of Nuclear Materials*, 414(3):399–407, 2011.

[45] R Pajarre. *Modelling of chemical processes and materials by free energy minimisation*. Phd thesis, Aalto University, 2016.

[46] P Koukkari and R Pajarre. Calculation of constrained equilibria by Gibbs energy minimization. *Calphad: Computer Coupling of Phase Diagrams and Thermochemistry*, 30(1):18–26, 2006.

[47] P Koukkari, R Pajarre, and P Blomberg. Reaction rates as virtual constraints in Gibbs energy minimization. *Pure and Applied Chemistry*, 83(5):1063–1074, 2011.

[48] P Gerdanian and M Dodé. Étude thermodynamique des oxydes UO_{2+x}. *J. Chim. Phys.*, 62:171–184, 1965.

[49] K Hagemark and M Broli. Equilibrium oxygen pressures over the nonstoicheiometric uranium oxides UO_{2+x} and U_3O_{8-z} at higher temperatures. *Journal of Inorganic and Nuclear Chemistry*, 28(12):2837–2850, 1966.

[50] K Kiukkola. High-temperature electrochemical study of uranium oxides in the UO_2-U_3O_8 region. *Acta Chem. Scand.*, 16:327–345, 1962.

[51] T B Lindemer and T M Besmann. Chemical thermodynamic representation of $UO_{2\pm x}$. *J. Nucl. Mater.*, 130:473–488, 1985.

[52] M H A Piro. *Computation of thermodynamic equilibria pertinent to nuclear materials in multi-physics codes. Ph.D. thesis.* PhD thesis, Royal Military College of Canada, Kingston, ON, Canada, 2011.

[53] B Cox. Environmentally-induced cracking of zirconium alloys - A review. *Journal of Nuclear Materials*, 170(1):1–23, 1990.

[54] P S Sidky. Iodine stress corrosion cracking of Zircaloy reactor cladding: iodine chemistry (a review). *Journal of Nuclear Materials*, 256(1):1–17, 1998.

[55] M H A Piro, D Sunderland, S Livingstone, J Sercombe, W Revie, A Quastel, K Terrani, and C Judge. A Review of Pellet–Clad Interaction Behavior in Zirconium Alloy Fuel Cladding. In *Reference Module in Materials Science and Materials Engineering*, pages 1–68. 2017.

[56] L. Desgranges, Ch Riglet-Martial, I. Aubrun, B. Pasquet, I. Roure, J. Lamontagne, and T. Blay. Evidence of tellurium iodide compounds in a power-ramped irradiated UO_2 fuel rod. *Journal of Nuclear Materials*, 437(1-3):409–414, 2013.

[57] K Konashi, T Yato, and H Kaneko. Radiation effect on partial pressure of fission product iodine. *J. Nucl. Mater.*, 116:86–93, 1983.

[58] K Konashi, M Yamawaki, and T Yoneoka. CsI decomposition due to collision cascade initiated by fission fragments. *Journal of Nuclear Materials*, 160:75–80, 1988.

[59] R G J Ball, W G Burns, J Henshaw, M A Mignanelli, and P E Potter. The chemical constitution of the fuel-clad gap in oxide fuel pins for nuclear reactors. *Journal of Nuclear Materials*, 167:191–204, 1989.

[60] V M Filin, V V Novikov, A S Sotnikov, S M Bogatyr', and V I Kuznetsov. Particulars of the Effect of the Internal Medium of a Fuel Element in High-Burnup Fuel on the Corrosion Cracking of Fuel-Element Cladding under Stress. *Atomic Energy*, 115(5):1–6, 2014.

[61] B J Lewis, W T Thompson, M R Kleczek, K Shaheen, M Juhas, and F C Iglesias. Modelling of iodine-induced stress corrosion cracking in CANDU fuel. *Journal of Nuclear Materials*, 408(3):209–223, 2011.

[62] T J van Reenen and W J de Wet. Equations for the computer computation of the kinetic energy distributions of fission fragments released from nuclear fuel surfaces by recoil. Technical Report PEL-198, Pelindaba, Pretoria, South Africa, 1970.

[63] K Konashi, Y Shiokawa, and H Kayano. Simulation of CsI decomposition in fuel cladding gap. *Journal of Nuclear Materials*, 232:181–185, 1996.

[64] IAEA. Design of the Reactor Core for Nuclear Power Plants. Technical Report NS-G-1.12, IAEA, Vienna, Austria, 2005.

[65] STUK. Radiation and Nuclear Safety Authority Regulation on the Safety of a Nuclear Power Plant, Regulation STUK Y/1/2018. 2018.

[66] STUK. Nuclear fuel and reactor, YVL B.4, 2013.

[67] K J Geelhood, W G Luscher, P A Raynaud, and I E Porter. FRAPCON-4.0: A computer code for the calculation of steady-state, thermal-mechanical behavior of oxide fuel rods for high burnup. Technical Report PNNL-19418, Pacific Northwest National Laboratory, 2015.

[68] K J Geelhood, W G Luscher, J M Cuta, and I A Porter. FRAPTRAN-2.0: A Computer Code for the Transient Analysis of Oxide Fuel Rods. Technical Report PNNL-19400, Vol. 1 Rev. 2, PNNL, Richland, WA, USA, 2016.

[69] A Moal, V Georgenthum, and O Marchand. SCANAIR: A transient fuel performance code: Part One: General modelling description. *Nuclear Engineering and Design*, 280:150–171, 2014.

[70] J D Hales, K A Gamble, B W Spencer, S R Novascone, G Pastore, W Liu, D S Stafford, R L Williamson, D M Perez, and R J Gardner. BISON Users Manual - BISON Release 1.1. Technical Report INL/MIS-13-30307 Rev. 2, Idaho National Laboratory, Idaho Falls, IA, USA, 2014.

[71] P Van Uffelen, J Hales, W Li, G Rossiter, and R Williamson. A review of fuel performance modelling. *Journal of Nuclear Materials*, 516:373–412, 2019.

[72] U Rohde. The modeling of fuel rod behaviour under RIA conditions in the code DYN3D. *Annals of Nuclear Energy*, 28(13):1343–1363, 2001.

[73] H Kim, C Shin, Y Yang, and T Kim. Development of fully coupled FRAPTRAN with MARS-KS code system for calculation of fuel behavior during LOCA. In *TopFuel*, Prague, Czechia, 2018. European Nuclear Society.

[74] G Grandi. SIMULATE5 fuel pin model description and verification against ENIGMA. In *TopFuel*, Prague, Czechia, 2018. European Nuclear Society.

[75] F Anselin. The role of fission products in the swelling of irradiated UO_2 and (U,Pu)O_2 fuel. Technical Report GEAP-5583, General Electric, Sunnyvale, California, 1969.

[76] G Pastore, L Luzzi, V Di Marcello, and P Van Uffelen. Physics-based modelling of fission gas swelling and release in UO_2 applied to integral fuel rod analysis. *Nuclear Engineering and Design*, 256:75–86, 2013.

[77] D D Baron and L Hallstadius. Fuel performance of light water reactors (uranium oxide and MOX). volume 1 of *Comprehensive Nuclear Materials*, pages 481–514. Elsevier, 2012.

[78] K J Geelhood and W G Luscher. Material property correlations: Comparisons between FRAPCON-3.4, FRAPTRAN-1.4 and MATPRO. Technical Report NUREG/CR-7024, Rev. 1, US NRC, 2011.

[79] R O Meyer. The analysis of fuel densification. Technical Report NUREG-0085, US NRC, Washington, DC, USA, 1976.

[80] K Lassmann, C O'Carroll, J van de Laar, and C T Walker. The radial distribution of plutonium in high burnup UO_2 fuels. *Journal of Nuclear Materials*, 208(3):223–231, 1994.

[81] P Blair. *Modelling of fission gas behaviour in high burnup nuclear fuel*. Phd thesis, École Polytechnique Fédérale de Lausanne, 2008.

[82] A R Massih and K Forsberg. Calculation of grain boundary gaseous swelling in UO_2. *Journal of Nuclear Materials*, 377:406–408, 2008.

[83] P Hermansson and A R Massih. An effective method for calculation of diffusive flow in spherical grains. *Journal of Nuclear Materials*, 304:204–211, 2002.

[84] J A Turnbull, C A Friskney, J R Findlay, F A Johnson, and A J Walter. The diffusion coefficients of gaseous and volatile species during the irradiation of uranium dioxide. *J. Nucl. Mater.*, 107:168–184, 1982.

[85] J A Turnbull, R J White, and C Wise. The diffusion coefficient for fission gas atoms in uranium dioxide. In *Water Reactor Fuel Element Computer Modelling in Steady State, Transient and Accident Conditions IWGFPT/32*, pages 174–181, Preston, UK, 1988. IAEA.

[86] R J White and M O Tucker. A new fission gas release model. *Journal of Nuclear Materials*, 118:1–38, 1983.

[87] P van Uffelen, G Pastore, V di Marcello, and L Luzzi. Multiscale modelling for the fission gas behaviour in the TRANSURANUS Code. *Nuclear Engineering and Technology*, 43(6):477–488, 2011.

[88] T Ikonen. VTT's modifications to the FRAPCON-4.0 code. Technical Report VTT-R-00119-17, VTT Technical Research Centre of Finland Ltd., Espoo, Finland, 2017.

[89] K Forsberg and A R Massih. Fission gas release under time-varying conditions. *Journal of Nuclear Materials*, 127:141–145, 1985.

[90] E Tenckhoff. Review of Deformation Mechanisms, Texture, and Mechanical Anisotropy in Zirconium and Zirconium Base Alloys. *Zirconium in the Nuclear Industry: Fourteenth International Symposium*, 2(4):25–25–26, 2008.

[91] T A Hayes and M E Kassner. Creep of zirconium and zirconium alloys. *Metallurgical and Materials Transactions A*, 37A:2389–2396, 2006.

[92] F Dunne and N Petrinic. *Introduction to computational plasticity*. Oxford University Press, 2005.

[93] K J Geelhood, W G Luscher, and C E Beyer. PNNL Stress / Strain Correlation for Zircaloy. Technical report, 2008.

[94] A Shestopalov, K Lioutov, and L Yegorova. Adaptation of USNRC's FRAPTRAN and IRSN's SCANAIR Transient Codes and Updating of MATPRO Package for Modeling of LOCA and RIA Validation Cases with Zr-1 % Nb (VVER type) Cladding. Technical Report NUREG/IA-0209, Moscow, Russia, 2003.

[95] A S Khan and S Huang. *Continuum theory of plasticity*. John Wiley & Sons, Inc., 1995.

[96] M Limbäck and T Andersson. A Model for Analysis of the Effect of Final Annealing on the In- and Out-of-Reactor Creep Behavior of Zircaloy Cladding. In *Zirconium in the Nuclear Industry (11th)*, pages 448–468. ASTM, 1996.

[97] K Geelhood. Implementing primary creep calculations during stress changes and reversals in the fuel performance code FRAPCON-3. In *TopFuel*, pages 188–194, Charlotte, NC, USA, 2013. ANS.

[98] M A McGrath. In-reactor creep behaviour of Zircaloy-2 under variable loading conditions in IFA-585. Technical Report HWR-471, HRP, Halden, Norway, 1996.

[99] S Watanabe. In-reactor creep behaviour of LWR fuel cladding, interim results up to 4th operational cycle. Technical Report HWR-926, HRP, Halden, Norway, 2010.

[100] M Zahoor. Modeling primary creep for Zircaloy claddings during load reversals and drops in BISON. *Journal of Nuclear Materials*, 511:212–219, 2018.

[101] OECD/NEA. International Fuel Performance Experiments (IFPE) database, 2017.

[102] K Lassmann, A Schubert, J Van De Laar, and P Van Uffelen. The 'Fuel Rod Analysis ToolBox': A general program for preparing the input of a fuel rod performance code. *Annals of Nuclear Energy*, 81:332–335, 2015.

[103] C Bagger, H Carlsen, and P Knudsen. Details of design, irradiation and fission gas release for the Danish UO_2-Zr irradiation test 022. Technical Report Risö-M-215, Risö, Roskilde, Denmark, 1978.

[104] L W Newman, T P Papazoglou, G M Bain, W A McInteer, T D Pyecha, P L Holman, and P C Aadland. The hot cell examination of Oconee 1 fuel rods after five cycles of irradiation. Technical Report BAW-1874, Babcock & Wilcox, Lynchburg, VA, USA, 1986.

[105] J A Turnbull. Concluding report on three PWR rods irradiated to 90 MWd/kg UO_2 in IFA-519.9: Analysis of measurements obtained in-pile and by PIE. Technical Report HWR-668, OECD Halden Reactor Project, Halden, Norway, 2001.

[106] C R Hann, J L Bates, D W Brite, J L Daniel, N C Davis, P E Hart, R K Marshall, G B Mellinger, and R E Williford. Test design, precharacterization, and fuel assembly fabrication for instrumented fuel assemblies IFA-431 and IFA-432. Technical Report NUREG/CR-0332, PNNL, Richland, WA, USA, 1977.

[107] T Tverberg and M Amaya. Study of thermal behaviour of UO_2 and $(U,Gd)O_2$ to high burnup (IFA-515). Technical Report HWR-671, OECD Halden Reactor Project, Halden, Norway, 2001.

[108] R Josek. The high initial rating test IFA-677.1: Final report on in-pile results. Technical Report HWR-872, OECD Halden Reactor Project, Halden, Norway, 2008.

[109] H K Jenssen and N O Solum. Post irradiation examination (PIE) on the test rods from the gadolinia fuel test in IFA- 681. Technical Report HWR-1094, OECD Halden Reactor Project, Halden, Norway, 2016.

[110] G Pastore, J D Hales, S R Novascone, B W Spencer, and R L Williamson. Modelling of the gadolinium fuel test IFA-681 using the BISON code. In *Enlarged Halden Programme Group Meeting*, page 14, 2016.

[111] William L Oberkampf, Sharon M Deland, Brian M Rutherford, Kathleen V Diegert, and Kenneth F Alvin. Estimation of total uncertainty in modeling and simulation. *Reliability Engineering & System Safety*, 75(April):333–357, 2002.

[112] M C Kennedy and A O'Hagan. Bayesian calibration of computer models. *Journal of the Royal Statistical Society: Series B (Statistical Methodology)*, 63(3):425–464, 2001.

[113] STUK. Deterministic safety analyses for a nuclear power plant, YVL B.3, 2013.

[114] J K Patel. Tolerance limits — A review. *Communications in Statistics - Theory and Methods*, 15(9):2719–2762, 1986.

[115] S S Wilks. Determination of Sample Sizes for Setting Tolerance Limits. *The Annals of Mathematical Statistics*, 12(1):91–96, 1941.

[116] S S Wilks. Statistical prediction with special reference to the problem of tolerance limits. *Annals of Mathematical Statistics*, (13):400–409, 1942.

[117] L Pál and M Makai. Remarks on statistical aspects of safety analysis of complex systems. 2002.

[118] R J A Little and D B Rubin. *Statistical Analysis with Missing Data*. John Wiley & Sons, Inc., Hoboken, NJ, USA, 2nd edition, 2002.

[119] D R Rubin. Inference and missing data. *Biometrika*, 63:581–592, 1976.

[120] L. Johnson, I. Günther-Leopold, J. Kobler Waldis, H. P. Linder, J. Low, D. Cui, E. Ekeroth, K. Spahiu, and L. Z. Evins. Rapid aqueous release of fission products from high burn-up LWR fuel: Experimental results and correlations with fission gas release. *Journal of Nuclear Materials*, 420(1-3):54–62, 2012.

[121] K Oldberg. Distribution of fission gas release in 10x10 fuel. Technical Report TR-09-25, SKB AB, Stockholm, Sweden, 2009.

[122] E Nordström. Fission gas release data for Ringhals PWRs. Technical Report TR-09-26, SKB AB, Stockholm, Sweden, 2009.

[123] C Vitanza, E Kolstad, and U Graziani. Fission gas release from UO_2 pellet fuel at high burn-up. In *LWR Fuel Topical Meeting*, pages 361–366, Portland, OR, USA, 1979. ANS.

[124] T Ikonen and V Tulkki. The importance of input interactions in the uncertainty and sensitivity analysis of nuclear fuel behavior. *Nuclear Engineering and Design*, 275:229–241, 2014.

[125] V Yu Mat'ev. Energy Deposition by Fission Fragments in Nuclear-Pumped Lasers: I. A General Method of Calculation. *Technical Physics*, 46(1):68–75, 2001.

[126] S Kahn, R Harman, and V Forgue. Energy Distributions of Fission Fragments from Uranium Dioxide Films. *Nuclear Science and Engineering*, 23(1965):8–20, 1965.

[127] D H Nguyen and L M Grossman. Ionization by Fission Fragments Escaping from a Source Medium. *Nuclear Science and Engineering*, 30:233–241, 1967.

Errata

Publication II

In the label of the second column in table 2, the first letter of the word *serpent* should be capitalized.

Publication III

The heading of section 6, *Acknoledgements*, should read *Acknowledgements*.

Publication IV

In the second and fourth paragraphs of section 3.2, *Zircalloy-4* should read *Zircaloy-4*.

Publication V

In the third paragraph, *curnup* should be replaced with *burnup*, and the words *Ikonen et al.* are duplicated.

Publication VI

In Eq. (6), variable n should be N.

Typical light-water reactor nuclear fuel consists of a ceramic uranium oxide pellet in a metallic zirconium cladding tube. The fuel undergoes various changes in its properties and composition as it is irradiated in a nuclear power plant. The effects of the composition change on the chemical properties are studied in this thesis with thermochemical modeling using Gibbs energy minimization. These models were validated and release of corrosive gases from the pellet also studied.

Thermomechanical changes in the fuel are studied with engineering-scale tools, such as the FINIX fuel behavior module developed at VTT. The temperature predictions of FINIX were improved in this thesis by implementing models for important phenomena that occur during long irradiation periods.

Finally, uncertainty analysis methods for fuel performance code fission gas release predictions were developed. Fission gas release can be correlated with the instant release fraction of certain radionuclides in spent fuel disposal. The instant release fraction is released relatively instantly as groundwater becomes in contact with the fuel after the disposal canister has failed. With an estimate of the uncertainty of the fission gas release predictions, the uncertainty of the instant release fraction can be studied in more detail.

Aalto-DD 22/2020

ISBN 978-952-60-8942-3 (printed)
ISBN 978-952-60-8943-0 (pdf)
ISSN 1799-4934 (printed)
ISSN 1799-4942 (pdf)

Aalto University
School of Science
Department of Applied Physics
www.aalto.fi

BUSINESS + ECONOMY

ART + DESIGN + ARCHITECTURE

SCIENCE + TECHNOLOGY

CROSSOVER

DOCTORAL DISSERTATIONS